2017

Water assisted laser heat treatment of polycrystalline cubic boron nitride tool materials

Kwang Shiong Wong
Iowa State University

Water assisted laser heat treatment of polycrystalline cubic boron nitride tool materials

by

Kwang Shiong Wong

A thesis submitted to the graduate faculty

in partial fulfillment of the requirements for the degree of

MASTER OF SCIENCE

Major: Mechanical Engineering

Program of Study Committee:
Pranav Shrotriya, Major Professor
Scott Chumbley
Abhijit Chandra

Iowa State University

Ames, Iowa

2017

TABLE OF CONTENTS

LIST OF FIGURES iv
LIST OF TABLES vi
ABSTRACT vii
CHAPTER 1: INTRODUCTION 8
1.1 Problem statement 8
1.2 Background 8
1.2.1 Material microhardness measurement 8
1.2.2 Ultrahard materials 9
1.2.3 Different types of lasers 10
1.2.4 Laser material interactions 12
1.2.5 Laser processing – deposition, machining, thermal shock, surface treatment 14
1.3 Research objectives 16
1.4 Experiment setup 17
1.4.1 CO_2 continuous wave laser water-jet system 17
1.4.2 Nd:YAG pulsed laser system 19
CHAPTER 2: HYBRID CO_2 LASER WATERJET HEAT (LWH) TREATMENT OF BINDERED BORON NITRIDE COMPOSITES WITH HARDNESS IMPROVMENT 20
Abstract 20
2.1 Introduction 21
2.2 Method 25
2.3 Results 29
2.4 Discussions 35
2.4.1 Microstructure of the sample before LWH treatment 36
2.4.2 Microstructure of the sample after LWH treatment 38
2.5 Conclusions 43
Acknowledgment 44
CHAPTER 3: HARDNESS CHANGE DURING WATER ASSISTED PULSED LASER HEAT TREATMENT OF POLYCRYSTALLINE CUBIC BORON NITRIED TOOL MATERIALS 45
Abstract 45
3.1 Introduction 46
3.2 Experimental detail 48
3.2.1 Laser system setup and dual-phase materials 48
3.2.2 Laser surface treatment 48

3.2.3 Measurement of micro-hardness 49
3.2.4 Investigation of micro-structure and phase composition 49
3.3 Experimental results 50
3.3.1 Visual examination 50
3.3.2 Micro-hardness test 51
3.4 Discussion 53
3.5 Conclusions 68
CHAPTER 4: CONCLUSIONS AND FUTURE WORKS 69
4.1 Conclusions 69
4.2 Future works 70
REFERENCES 71

LIST OF FIGURES

Figure 1: Regimes of various effects during laser–material interactions and their application [13] 13
Figure 2: Laser head of CO_2 continuous wave laser water-jet system..... 18
Figure 3: Laser and gas outlet and water outlet 18
Figure 4: Nd:YAG pulsed laser system..... 19
Figure 5: Schematic of LWJ heat treatment process..... 28
Figure 6: Comparison of compressed air and nitrogen LWH treated results..... 30
Figure 7: SEM micrograph of LWH treated BN composite 30
Figure 8: SEM micrograph of cBN showing color change in LWH-treated area..... 31
Figure 9:SEM images of the indentations: (left) untreated and (right) LWH treated dual phase cBN/TiN..... 32
Figure 10: LWH treated 55%cBN/45%TiN material hardness change ratio 33
Figure 11: LWH treated 82%cBN/18%TiN material hardness change ratio 33
Figure 12: LWH treated pure cBN material hardness change ratio 34
Figure 13: LWH treated pure cBN material hardness change ratio as a function of distance from laser beam center..... 34
Figure 14: Surface condition of LWH treated 30 passes area of 82%cBN/18%AlN composite 36
Figure 15: SEM micrograph showing microstructure of untreated 82%cBN/18%AlN sample 37
Figure 16: SEM micrograph showing microstructure of untreated 55%cBN/45%TiN sample 38
Figure 17: SEM micrograph showing the LWH-treated microstructure of cBN/AlN composite 39
Figure 18: SEM point analysis of LWH treated cBN/AlN composite..... 41
Figure 19: SEM image of LWH treated cBN/TiN composite..... 42
Figure 20: EDS line analysis of LWH treated cBN/TiN composite 43
Figure 21: Comparison between untreated area and treated area (top:82% cBN, bottom: 55% cBN)..... 50
Figure 22: SEM images showing microstructure of untreated 82% cBN area. 55
Figure 23: SEM images showing microstructure of 82% cBN after laser heat treatment: 8 passes 55
Figure 24: SEM images showing microstructure of 82% cBN after laser heat treatment: 16 passes 56
Figure 25: SEM images showing microstructure of untreated 55% cBN area 57
Figure 26: SEM images showing microstructure of 55% cBN after laser heat treatment: 4 passes 57
Figure 27: SEM images showing microstructure of 55% cBN after laser heat treatment: 16 passes 58
Figure 28: Untreated and treated areas selected for grain size analysis 59
Figure 29: Hardness increase ratio vs. numbers of particles increase ratio (82% cBN)..... 61
Figure 30: Hardness increase ratio vs. numbers of particles increase ratio (55% cBN)..... 61
Figure 31: The relationship between hardness change and diameter change in Hall-Petch

relationship 63
Figure 32: Comparison between untreated area and 2x2 mm treated area (top: 82% cBN, bottom: 55% cBN) 64
Figure 33: Raman spectrum of untreated 82% cBN 65
Figure 34: Raman spectrum of heat treated 82% cBN 66
Figure 35: Raman spectrum of untreated 55% cBN 67
Figure 36: Raman spectrum of treated 55% cBN 67

LIST OF TABLES

Table 1: Nd:YAG laser specifications (wavelength=532nm) 19
Table 2: Properties of selected hard materials 23
Table 3: LWH treatment parameters 27
Table 4: Calculated grain size of BN composites 40
Table 5: 82% cBN heat treatment with and w/o water 51
Table 6: cBN heat treatment with and w/o water 52
Table 7: Hardness increase ratio of 2x2 area 53
Table 8: Grain size of 82% cBN 60
Table 9: Grain size of 55% cBN 60

ABSTRACT

This thesis explores a new development in improving the surface properties to ultrahard material using a variety of laser systems, which are CO_2 continuous wave laser water-jet system and Nd:YAG pulsed laser system. Two different types of cBN materials were used, which were bindered 82%cBN/18%AlN and 55%cBN/45%TiN. In the heat treatment using the CO_2 continuous wave laser water-jet system, the effects of different types of gases, number of laser beam passes, and distribution of laser power were studied. In addition, in the heat treatment using the Nd:YAG pulsed laser system, the effects of quenching and number of laser beam passes were studied as well. In both studies, the hardness was investigated using Knoop hardness measurement, and the microstructures of the sample surfaces were characterized using Scanning Electron Microscope (SEM).

CHAPTER 1: INTRODUCTION

1.1 Problem statement

In manufacturing, producing materials always includes the processes of cutting, abrasive and drilling. The machining and abrasive tools have to be hard enough to guarantee the sufficient effectiveness, otherwise the tools will easily get fatigued and fracture after the manufacturing processes.

How can the problems of fatigue and fracture be reduced or avoided from the manufacturing processes?

First of all, superhard materials can be used as the manufacturing tools, since its superior mechanical properties can increase the number of cycles that will cause fatigue of manufacturing tools. Furthermore, some mechanical processes can be used to increase the hardness of superhard materials, such as laser heat treatment.

1.2 Background

1.2.1 Material microhardness measurement

According to the Metal Handbook, hardness is defined as “resistance of metal to plastic deformation” [1]. Hardness is the property of a material's and its resistance to cutting, abrasive, and scratching [2]. Indentation hardness is one kind of hardness test. When a rounder or pointed indenter is pressed into the material surface, an indentation is made for hardness measurement. Microhardness testing is one kind of indentation hardness test. An applied load, which is 1 kg or less, is used for a static force to the indenter to make a small indentation, which can be as

small as 0.0125 mm in length [2]. Vicker hardness test is one the most common microhardness test. The diamond indenter used in the Vickers hardness test is a square-based pyramid and has a 136º angle different between opposite sides. Other than Vickers hardness test, Knoop hardness test is also commonly used for microhardness measurement. The indenter used in Knoop hardness test is a pyramid-shaped diamond indenter with apical angles of 130º and 172º. The advantages of both hardness tests are that an accurate reading in hardness can be taken and the hardness of all the materials softer than diamond can be measured.

1.2.2 Ultrahard materials

Only polycrystalline diamond and polycrystalline cubic boron nitride (cBN) can be considered ultrahard materials on earth because the Vickers hardness of those two materials is greater than 35 GPa [3]. They have high thermal conductivity and the same cubic crystallographic structure.

Polycrystalline diamond can be considered the hardest material on earth and is found in nature. Due to its high hardness, diamond is commonly used in industrial cutting and has 50-200 longer tool lives than the other carbide cutting tools. However, diamond is only used for non-ferrous materials because diamond reacts with iron at a high cutting temperature [3].

Polycrystalline cubic boron nitride (cBN) is the hardest material after diamond. Unlike diamond, cBN is an artificial material and cannot be found in nature [4]. cBN is produced from the conversion of hexagonal boron nitride (hBN) under the conditions of high pressure (4-7 Gpa) and high temperature (1730-3230 °C) [5]. In industrial cutting, cBN is more popular than diamond because of its thermal stability. cBN is still stable in air and vacuum at a temperature of 1550 °C, whereas diamond starts to form a graphite surface layer at the temperature between

650 °C under the condition of surrounding oxygen[4].

Besides diamond and cBN, Cook claimed that aluminum magnesium boride (AlMgB14) can be also considered as ultrahard material. AlMgB14 can be also called BAM and it Vicker's hardness was reported to be 32 GPa. After combining with titanium diboride (TiB2) in hot pressing, and the Vicker's hardness of BAM was reported to be greater than 40 GPa [6].

Some materials can be chosen to be potential ultrahard material because their hardness is close to ultrahard materials. Ulrich deposited a boron carbide (B4C) layer under the condition of room temperature and its hardness was reported to be 30 GPa [7]. Other than that, Basu reported that monolithic TiB2 based materials reached a hardness of 25 GPa. TiB2 can be combined with the other ultrahard materials to increase its hardness [8].

1.2.3 Different types of lasers

Continuous wave (CW) laser is the most common type of laser used in the research field. CW laser means the laser continuously emits beam light at a certain frequency. The first continuous wave laser invented by Theodore H. Maiman in 1960 at Hughes Research Laboratories in Malibu, California. Maiman used a cylinder of synthetic ruby with the ends silver-coated to make the laser reflective, and photographic flashlamps were used as the pump source [9]. In the same year, Sorokin and Stevenson promoted the Uranium laser, which was a four-stage solid-state laser, and Javan, Herriott, and Bennet invented Helium Neon laser, which was the first continuous wave laser operating at the wavelength of 1153 nm. Besides Uranium and Helium Neon lasers, Carbon Dioxide laser (CO_2 laser) is also one of the most useful lasers in the world [10]. Patel, the inventor of CO_2 laser, demonstrated CW laser action on vibrational

transitions of the vibration band of CO_2 at the wavelength of 9.4 and 10.4 um. The mixture gas in the discharge tube is filled with carbon dioxide, nitrogen, hydrogen and xenon. The average power of a laser beam generated by a CO_2 laser can reach more than 6000 W. Due to its high power output, the CO_2 laser can be used for machining, welding, and heat treatment. The power density of a CW laser is calculated using the following equation (1):

$$\text{Average power density} = P/A \quad (1)$$

P: power of the laser beam

A: Area of the laser beam spot

Pulsed laser is another useful type of laser in research field. The condition of a pulsed laser depends on the repetition rate, peak power, and pulse duration. Repetition rate is the number of emitted pulses per second, which is known as frequency. For example, 1 GHz repetition rate means 1 giga pulses generated in a second. Pulse duration is the duration of a pulse since generated to the end. For example, the pulse duration of a nanosecond laser beam is within 1-999 nanoseconds. Due to the short pulse durations, the peak power of the pulsed laser is much higher than the average power of CW laser and the peak power can be calculated using the following equation:

Peak power = pulse energy/pulse duration.

Since the pulse duration can be in nanoseconds, picoseconds, and femtoseconds, the peak power of a pulsed laser can be calculated to be in gigawatt, terawatt, and petawatt. The high peak power generation by pulsed lasers creates nonlinear heat absorption to materials. Nd:YAG laser is one most of common lasers used in the world.

The main difference between these two mainstream lasers is that pulsed lasers produce an incredibly high peak power over the average power generated by CW lasers (petawatt vs.

kilowatt). Other than the power, the CW laser creates a large heat-affected zone to the material because the heat of the laser beam transfers continuously throughout the entire material. On the other hand, the pulses of pulsed lasers end in a short duration and the heat is not able to transfer too far from the heat source, so the heat affected zone is small. According to Liu, pulsed lasers gave a small heat-affected zone over CW lasers in micromachining [11]. Furthermore, he also compared the micromachining results from two different pulse width lasers and found that the shorter pulse width laser caused the treated area to be more uniform and less cracks on the material surface. However, in the other situation, CW lasers may produce a better heat treatment result. For example, Kumpulainen used a pulsed fiber laser and a continuous wave diode laser to sinter silver nanoparticles, separately [12]. Since evaporating the additives requires heat, Kumpulainen stated the pulsed laser beam sintered the materials too quick and the inconsistent peak power of the pulses caused porous structure on the surface materials. Even though the CW laser caused a large heat affected zone, on the other hand, it promised that the heat could transfer throughout the entire sample consistently. Therefore, different types of lasers guarantee the different manufacturing processes.

1.2.4 Laser material interactions

According to Dahotre, when the laser beam irradiates on a material surface, phenomena of reflection, absorption, refraction, scattering, and transmission occur. Absorption and reflection of radiation are the most interesting phenomena in the laser processing of materials. In general, a material's reflection increases and absorption decreases with increasing wavelength. Therefore, the materials become more absorbing at a shorter wavelength. In additions, the absorption and reflection in the laser processing of materials also depend on the

temperature. At a higher temperature, the material becomes more absorbing. The regimes of various laser material interactions were also studied by Dahotre and shown in Figure 1. This figure showed the relationship of laser light intensity and the interaction time between the material and laser beam. Surface modifications, as known as surface heat treatment, need an intensity of about 10e8 W/cm^2 and a interaction time of about 10e-9 to 10e-7 s. Q-switched Nd:YAG and UV excimer lasers are the most suitable for the laser processing of surface modifications. On the other hand, pulsed laser ablation (PLA) required a high laser intensity and short interaction time. Compared to surface modifications and PLA, in the laser processing, welding needs the lowest laser intensity and longest interaction time.

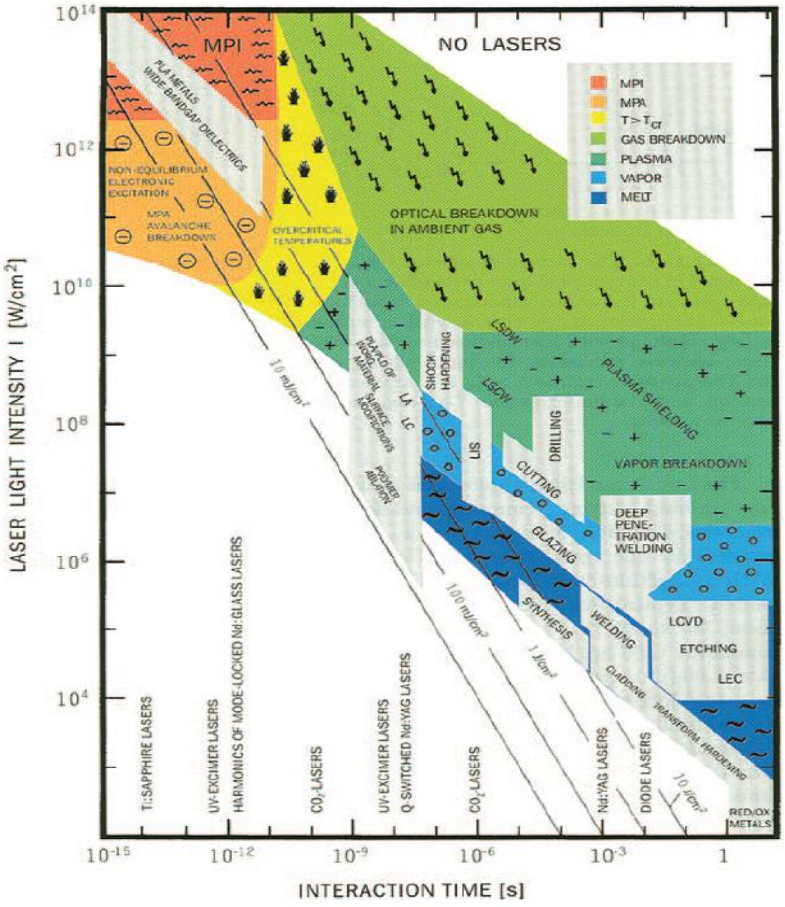

Figure 1: Regimes of various effects during laser–material interactions and their application *[13]*

1.2.5 Laser processing – deposition, machining, thermal shock, surface treatment

The laser is being commonly used in research and industry for over half a decade. Many manufacturing processes involve the laser, such as deposition, machining, shock peening, and surface treatment.

Deposition:

Pulsed laser deposition (PLD) is a physical vapor deposition technique. According to Willmott, high energy laser pulse is focused on the material surface, which is called the target. Above a certain power density, a feature of plasma is ablated, which was called plume, on the target material. The plume recondenses on a substrate and a thin film is grown at this point. Willmott also stated that PLD was better than the normal deposition because the film growth rate could be controlled to any desired amount and almost all metal and non-metal targets could be ablated using proper laser parameters [14].

Machining:

Perry stated that conventional mechanical lathes and machine tools are able to melt the materials down at a width of 200 um and a depth of 1 mm. Laser machining is expected to make finer features and irregular shape [15]. The conventional lasers, such as CO_2, copper vapor and Nd:YAG lasers, were not able to reach higher precision to all materials because of high thermal stress and large heat-affected zone. On the other hand, the ultraviolet lasers (less than 10 ps pulse width) could reach the negligible heat-affected zone and high precision in the laser machining process. The depth could be limited up to 0.5 um for both metals and non-metals [15]. Since continuous wave lasers caused a large heat-affected zone and thermal

damage to the material, Melaibari used a hybrid CO_2 laser-water-jet system (LWJ) to overcome those deficiencies. In this system, a CO_2 laser beam was followed by a high pressure water to machine polycrystalline cubic boron nitride (cBN). Furthermore, the effects of different fluid media (argon, nitrogen, oxygen, dry air, and water) were investigated [16].

Shock peening:

By generating minimal cold work, the laser shock peening (LSP) conducts compression to yield the material by using pulse lasers. In LSP, the high power laser beam focuses high energy pulse on a coating, such as black paint, black tape, and aluminum foil to generate the thermal shock. A layer of confining medium, such as water, glass slide, and quartz, is covered on the surface of the coatings. Since the compression is caused by the shock with cold work, the ultra-high heat generated by laser beam does not damage the material. The advantages of by LSP are that it strengthens material surfaces, decreases material fatigue, and makes powdered metals more compact. According to Cheng, by using LSP process, plastic deformation was found in silicon crystal. Large compressive residual stress was measured using Raman analysis and strong dislocation was characterized in TEM [17]. Molian applied LSP in additive manufacturing process, which was also called 3D printing. By using a high energy Q-switched Nd:YAG laser, nanoscale diamond powder was sintered. Molian also stated that LSP could limited the problems of porosity, rough surface, and shrinkage [18]. Baerga has done some experiments on different types of ZrO2 powder with using some different types of coatings and confining layers. A 64% hardness increase was reported on ZrO2 powder in mirco-scale by using water and black paint [19]. According to Lim, by using LSP, the number and size of corrosion pits on wear track of duplex stainless steel were reduced about 50%

compared to the untreated areas in the acetic acid salt spray test. Furthermore, a hardness increase was found in different levels of laser pulse densities [20].

Surface treatment:

In laser surface treatment, the laser radiation penetrates a thin layer on the top layer of the material. Advantages of surface treatment include an increase in hardness, improvements of wear resistance, and changes in structure. Mondal studied the effects of the laser surface treatment on corrosion and wear resistance on magnesium alloy. After the laser treatment, corrosion resistance improved due to microstructure refinement, absence of a new phase, and extended solid solubility [21].Besides corrosion and wear resistance, Badekes reported the hardness change on the titanium specimens. After the laser treatment, by using a KrF excimer laser, the surface of the treated area showed dark and white stripes and significant increase in hardness [22]

1.3 Research objectives

The purpose of this research effort is to investigate the effects of the heat treatment processes in cubic boron nitride by using continuous wave and pulsed lasers. The hardness and microstructure of the material surface before and after the laser heat treatment are studied. Since cBN play an important role in industry cutting and surface coating, the hardness of cBN becomes a critical properties. The microstructure gives clues about the hardness increase in cBN. According to Hall-Petch effect, the decrease of crystallite size and and dislocation in grains cause an increase in hardness of the ultrahard materials [23].

The hypothesis of the approach of this research is that the laser heat treatment affect the hardness due to the change in microstructure in the samples of cBN.

Hence the research objectives of this thesis are:

1. Demonstrate the feasibility of heat treatment to cBN samples using CO_2 and Nd:YAG lasers
2. Determine the hardness in the untreated and treated areas and study the mechanisms of hardness increase
3. Investigate the microstucture of the cBN sample using Scannning Electron Microscope (SEM).

1.4 Experiment setup

Two laser systems, laser water-jet and pulsed laser, were used for conducting the experiments.

1.4.1 CO_2 continuous wave laser water-jet system

In order to achieve a quenching effect, a novel process combining a continuous wave CO_2 laser and a water-jet was developed in our group to ensure the quality of machining cBN [24]. The laser water-jet system includes a 820 Spectra Physics continuous wave CO_2 laser (1064 nm wavelength and 1500 W power) and a water-jet setup. Shown in Figure 2, the laser head of the water-jet system was modified to accommodate the low-pressure waterjet, which is 1000 psi or 8 MPa. A focal spot diameter of 0.2 mm was produced using a 27 mm focal length lens, which was placed in the laser head. By adjusting the distance between the surface of the sample and laser head, a defocused spot could be received. The x-y positions could be

controlled by using a CNC controller. Shown in the Figure 3, three nozzles with different spacing of 2, 4, and 6 mm between the laser & gas outlet and water spray hole could be switched. The low pressure water spray followed the high laser power beam.

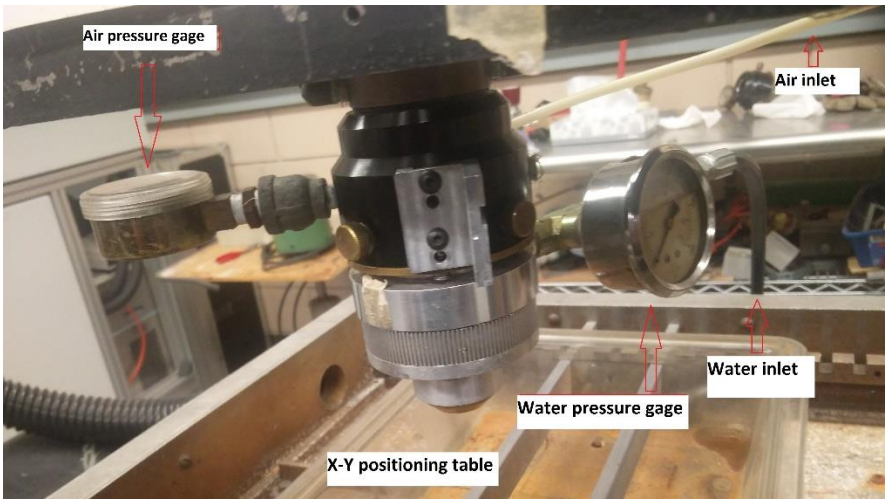

Figure 2: Laser head of CO_2 continuous wave laser water-jet system

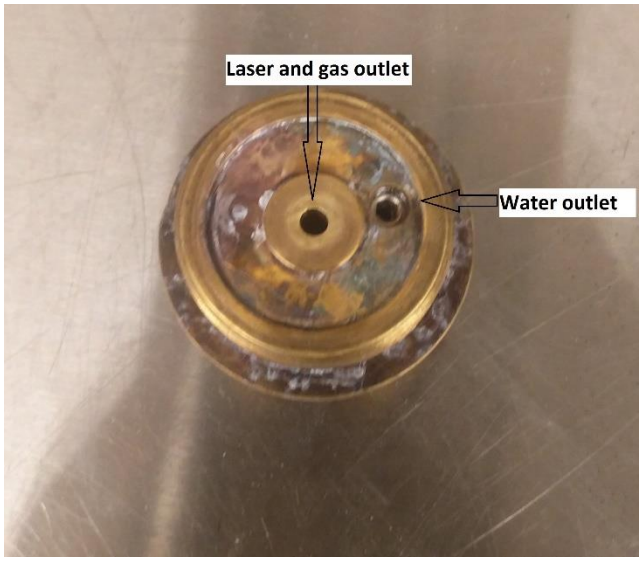

Figure 3: Laser and gas outlet and water outlet

1.4.2 Nd:YAG pulsed laser system

Figure 4 shows the Nd:YAG laser setup, which includes a Quanta-Ray INDI-30 Pulsed Nd:YAG nanosecond laser , a 45° reflective mirror, a focus lens, and 2D-motion stages.

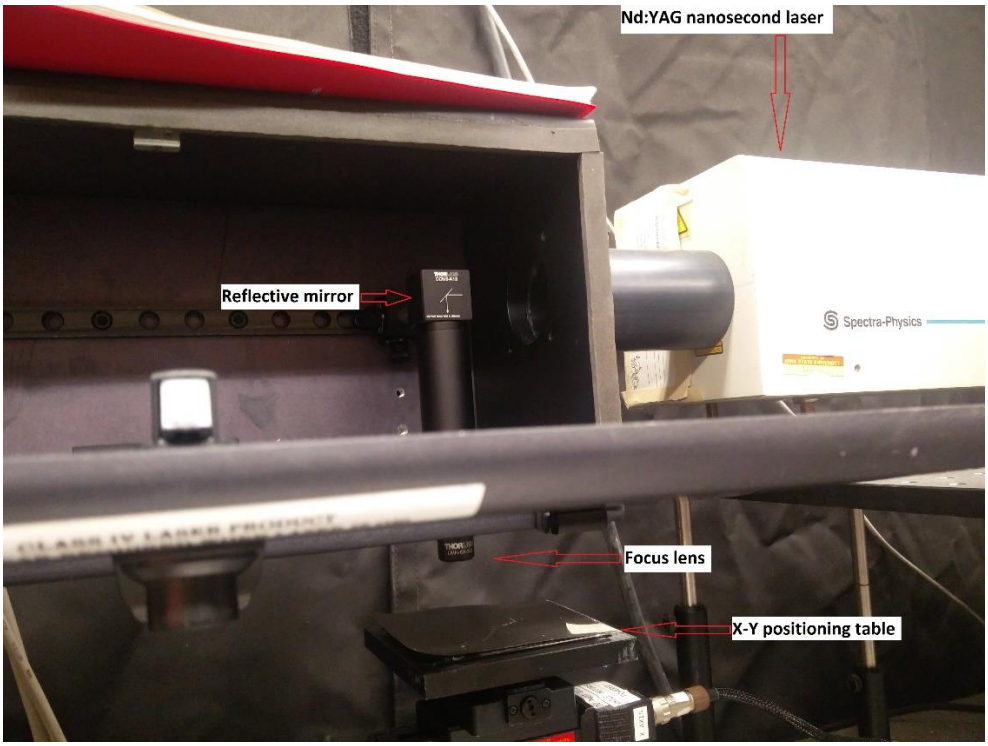

Figure 4: Nd:YAG pulsed laser system

This Nd:YAG laser was originally working in the wavelength of 1064 nm. However, after a harmonic generator was added, this laser could also work in the wavelength of 532 nm. The relationship between the laser powers under different repetition rates is shown in Table 1.

Table 1: Nd:YAG laser specifications (wavelength=532nm)

Frequency (Hz)	1	5	10
Power (W)	0.02	0.12	0.25

CHAPTER 2: HYBRID CO_2 LASER WATERJET HEAT (LWH) TREATMENT OF BINDERED BORON NITRIDE COMPOSITES WITH HARDNESS IMPROVMENT

A paper accepted for publication in *the journal of Ceramics International*

(2017)

Jingnan Zhao[1,2], Kwang Shiong Wong[3,4], Pranav Shrotriya[3,4]

Abstract

Boron nitride (BN) material is chemically and thermally stable which makes it desirable for high- speed machining in demanding chemical and thermal environments. Although the hardness of BN material is well below that of single polycrystalline diamond, a laser waterjet heat (LWH) treatment process provides a new potential approach to achieve hardness values that are comparable to diamond hardness. This study investigates the hardness change of LWH-treated bindered cBN/TiN and cBN/AlN composites. Results indicate that measured hardness increase is dependent on the laser beam pass and the distance from the beam center.

[1] Mechanical Engineering College, Tianjin University of Science and Technology, Tianjin, 300222, China
[2] Primary researcher and lead-author
[3] Department of Mechanical Engineering, Iowa State University, Ames, IS 50011, USA
[4] Co-author

2.1 Introduction

Hardness is defined as a material's resistance to a certain pressure given by the ratio of an applied load to the fully developed plastically area [25]. Diamond is considered to be the hardest material on earth whose hardness varies between 70 and 100 GPa depending on the quality and purity of the crystal. Compared to diamond's hardness, superhard materials are classified as having hardness values greater than 40 GPa [26]. Diamond ($H_k \approx 70 - 100$ GPa) and cubic boron nitride (cBN with $H_k \approx 40 - 50$ GPa) are well-known superhard materials that are used in many applications, such as mechanical cuttings, abrasives, polishing materials, and wear-resistant and protective coatings.

Although diamond is the hardest material, it also has limitations in the tooling industry. Due to its chemical instabilities, diamond is not an ideal tool for cutting ferrous materials because it reacts with ferrous materials to produce iron carbide. Also, diamond is not effective at high temperatures because of its thermal instability. On the other hand, cubic boron nitride (cBN), the second hardest material on earth [23], has a similar microstructure as diamond and it can be used to cut ferrous metals and perform in high temperature environments. Although cBN has good mechanical properties, chemical inertness and thermal stability, it cannot replace diamond as its hardness is well below that of diamond. Thus, searching for new superhard materials is not only of great scientific interest, but also of great practical value.

In order to find the most effective superhard materials for tooling industry, we should know the mechanisms that harden the materials. Diamond has a short bond length made of carbon atoms linked together in a face-centered cubic (FCC) lattice structure to form a three-dimensional high symmetry network. Each carbon atom is linked with four other carbon atoms in regular tetrahedrons, creating a cubic lattice with tremendous strength in all directions that

forms an incredibly solid crystal structure [27]. In addition, the bond length is short as carbon is the light element [28]. Thus, when we look for the superhard materials, light elements, such as boron, carbon, and nitrogen are considered. These elements are capable of forming three-dimensional rigid lattices with shortened covalent bonds. Moreover, in order to guarantee the material resistance to squeeze, the elements with very high densities of valence electrons should also be considered. With these ideas, the search for new superhard materials can be focused on the range of synthesized materials composed of light elements.

According to the ideas discussed above, some hard materials can be selected as potential superhard materials including cubic boron nitride [29], wurtzite boron nitride (wBN) [30], boron carbide (B4C) [14, 31], and titanium diboride (TiB2) [32, 33]. Table 2 shows the Knoop hardness, thermal stability, and chemical stability of those hard materials. Diamond has the highest hardness but the lowest oxidation temperature. Thus, diamond is unable to cut materials under high speed since the heat created by cutting could oxidize the diamond to carbon. cBN and wBN have high chemical inertness and high oxidation temperature that allow for high-speed manufacturing in various environments. Some researchers are working to improve the hardness of ceramic materials, such as boron carbide (B4C), tianium diboride (TiB2), and osmium diboride (OsB2), in order to reach the hardness of diamond. Thévenot increase the hardness B4C to 30 GPa at room temperature [14]. Gou and his group studied OsB2 and measured its hardness to be only 37 GPa [34]. Thus, OsB2 and B4C could not be considered as potential superhard materials to reach diamond hardness.

Table 2: Properties of selected hard materials

Synthetic materials	**Formula**	**Hardness (Knoop GPa)**	**Oxidation temperature in air (°C)**	**Chemical stability**
Polycrystalline Diamond	PCD	70-100	700	Reactive with ferrous materials
Cubic boron nitride	CBN	40-50	1300	High chemical inertness
Titanium diboride	TiB2	30	1100	High chemical inertness
Boron carbide	B4C	30	1400	High chemical inertness
wurtzite boron nitride	WBN	30	1200	High chemical inertness
Titanium nitride	TiN	21	800-900	High chemical inertness

Despite most previous works' efforts to create superhard materials by synthesizing superhard materials, many opportunities still remain unexplored. According to Hall-Petch effect, a decrease of crystallite size in randomly oriented polycrystalline materials results in an increase of the hardness due to the decrease of dislocation activity in grains [23, 25]. Dubrovinskaia's group measured a maximum load-invariant hardness of 85 GPa and a high fracture toughness of 15 MPa√m in cBN composites having nanoscale grain sizes (14 nm)

coupled with the formation of dense hexagonal and cubic BN phases structures within the grains [35]. The size effect of BN nanocomposites at 14 nm is the point at which the hardness increases due to stifled dislocation activity inside grains through the Hall–Petch effect and leveling off of plastic resistance due to increasing grain boundary shear [36]. In order to achieve this kind of superhard material, a novel laser/waterjet heat treatment (LWH) approach was performed on cBN/wBN composites. A preliminary study concluded that the hardness of the composition of cBN/wBN was comparable to the hardness of diamond [30, 37] .

The hybrid LWH process allows elements of the laser and waterjet treatment to be synergistically combined in a way to reveal the thermal shock-assisted fracturing of particles into microstructure refinement, rather than the melting and solidification of surface material to accomplish material processing. The LWH process consists of a low-power laser (160 W – 400 W) for precise heating of a small processing zone (1 mm width) on the workpiece. The laser heating will create a temperature gradient in the treated zone, and rapid waterjet quenching of the zone will develop thermal stresses that fracture the large particles which break into smaller particles, within the treated zone [38].

The effects of different environmental gases in laser cutting were also studied. Chen reported that nitrogen was a better environmental gas for cutting mild-steel plates, compared to air. Nitrogen-assisted laser cutting contributed to better dross adhesion and better roughness to the sample surface [39]. Melaibari, on the other hand, performed an experiment to investigate the material removal mechanisms in laser machining under different environmental gases and found that nitrogen-assisted machining caused deeper cutting but rougher cracked areas to the sample of cBN, compared to air-assisted machining [40]. Therefore, the environmental gas plays an important role in the heat transfer of laser beams.

The new discovery of rapidly quenched cBN/wBN composites with hardness values approaching those of diamond can have vast implications in the tooling industry. Hence, in this paper, a series of experiments on laser heat-treated dual phase cBN/wBN tools was designed in order to identify the fundamental phase transition and microstructure refinement features that contribute to the hardness improvements.

In previous studies [30, 37], the relationship among laser fluence, laser beam overlap percentage and hardness improvement was evaluated. Their test results showed that low laser fluence was a better choice because it could improve the hardness of cBN/wBN composites without damaging the sample, and a laser beam overlap of around 50% created the highest hardness improvement. However, the hardness improvement mechanism is still not clear since the hardness change ratio is not uniform throughout the laser beam track. Thus, a new experiment was designed for the study of laser/waterjet heat-treated cBN/wBN composites in order to find the effect of the environmental gases, the number of laser beam passes and laser power distribution on resulting hardness values.

2.2 Method

A continuous wave CO_2 laser (Spectra Physics 820) was employed to conduct the experiments with the laser parameters shown in Table 2. Four factors were studied in this paper: environmental gases, laser pass numbers, location of the laser beam track, and materials composition.

The first factor was the effects of different environmental gases on the material. As mentioned in the introduction, using different gases as assisted gases may influence the quality of the sample after the heat treatment. In this factor, two parameters, which were compressed

air and nitrogen gas, were applied only to the sample of 82%cBN/18%AlN. The environmental gas that performed best was chosen for the other samples that were used in the following experiments.

The second factor was the laser pass number. In previous studies, experiments were designed to find the relationship between material hardness change and the laser beam overlap [41]. With different laser beam overlaps, the boron nitride (BN) material hardness change ratio varied. Therefore, the multiple beam passes occur in the same location as the BN material that may enhance surface hardness. The following six levels of laser beam passes were tested in this study: 1, 2, 4, 8, 16, and 30 passes. The laser beam used in this study was a Gaussian beam, so the power density was not uniform along the entire beam path. Therefore, the laser beam energy irradiated on the cBN/wBN composite was not uniform along the width of the laser beam.

The Gaussian profile of the laser beam was approximated as a surface heat source whose intensity at radial distance r from center is given in Eq. (2):

$$\mathrm{I(z)} = a_s I_0 \exp\left(\frac{-2r^2}{w^2}\right) \tag{2}$$

where I_0 is the intensity at the center of the beam, a_s is the absorption coefficient, and w is the diameter of the laser beam spot. The absorption coefficient was chosen to be 0.75 [30]. Thus, the distance of the laser beam track from the center of the beam was set as the third factor.

Five levels of the distance from the laser beam center were designed in this paper: 50, 150, 250, 350, and 450 micrometers. The fourth factor is the boron nitride material's composition. Three kinds of commercial materials were used in this study: dual phase pure cBN, 82%cBN/18%AlN and 55%cBN/45%TiN. The average hardness of 100% cBN,

82%cBN/18%AlN and 55%cBN/45%TiN composites was 51 GPa, 46 GPa and 34 GPa respectively.

Table 3: LWH treatment parameters

Material	**Laser power (W)**	**Scanning speed (inch/min)**	**Waterjet pressure**	**Gas**
82%cBN/18%AlN	290	100	400 KPa	Pure Nitrogen
82%cBN/18%AlN	400	100	400 KPa	Compressed air
55%cBN/45%TiN	220	140	400 KPa	Compressed air

Similarly to our previous experiments, the experiment in this paper consisted of 3 steps. First, the heat treatment experiment was conducted by using a continuous wave CO_2 laser beam of 1 mm spot size with a speed of 140 inch/min and 100 inch/min (table 3). A low laser power was used to prevent melting, scribing or cutting of boron nitride. A waterjet stream immediately followed the laser beam, shown in Figure 5. The distance between the laser beam and waterjet is 0.062 inch. Thus, the time lags between them are 0.00045 s and 0.00062s, respectively.

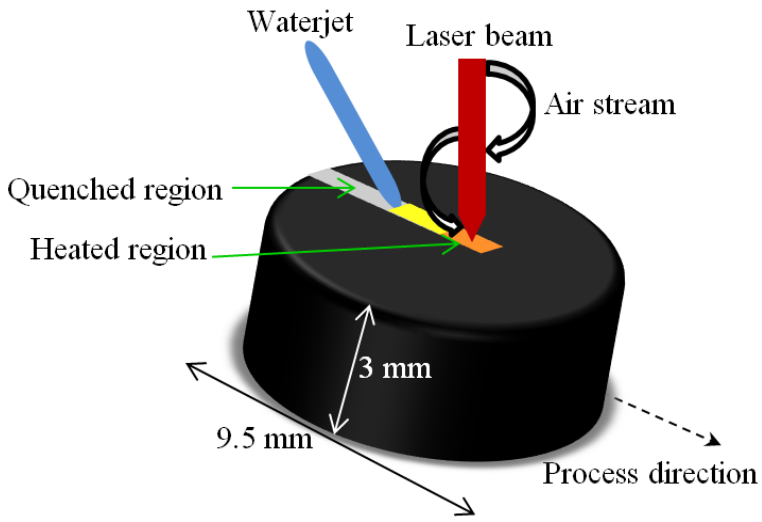

Figure 5: Schematic of LWJ heat treatment process

Second, in order to identify the change of the sample's hardness and toughness, Knoop microhardness tests were taken before and after LWH treatment. Indentation hardness tests were performed using a Tukon microhardness tester with a Knoop diamond pyramid indenter. The load was set at 0.5 kgf (4.9 N) and the test duration was set at 30 seconds. Length measurements were made along the long axis of the indentations using a high-resolution (± 0.4 μm) optical microscope and optical profilometer to ensure that no fracture had occurred in the indentation zone. Knoop hardness was then calculated using the relationship [29]:

$$HK = \frac{P}{C_p L^2} \tag{3}$$

where P is the load (kgf), C_p is the correction factor related to the shape of the indenter (0.070279 in this case) and L is the length of indentation along its long axis. In order to maintain precision while measuring the length of indentations, the indentation optical images were taken by optical microscope. The length of indentations was measured on an optical images by a Java-based image processing program known as ImageJ.

Third, a detailed microstructure analysis of both untreated and LWH treated samples were done using a FEI Quanta 250 FE-SEM. The SEM was operated in high vacuum mode, which provides better resolution than low vacuum mode. The BN samples were coated with a 2 nm-thick conductive iridium layer to reduce sample charging in the SEM. Secondary electron (SE) and backscattered electron (BSE) imaging were used to obtain images of different areas on the sample surface. The BSE images provide compositional contrast if the specimen has features with different composition [42]. Thus, this paper used BSE images to analyze the microstructural change before and after the LWH treatment of boron nitride samples. EDS was used to identify the specific elements on certain areas by using dot mapping, point analysis, and line analysis.

2.3 Results

As shown in Figure 6, the hardness change ratio using compressed air as the assisted gas was higher than the results using nitrogen as the assisted gas. In the heat treatment with compressed air, the highest hardness increase ratio, up to 30%, was found in the sample of bindered 82%cBN/18%AlN. In contrast, the maximum hardness increase ratio, up to 15%, was found locating at 150 microns from the center of the beam track in the heat treatment with nitrogen gas. Except with 1-pass treatment, the experiments with nitrogen as assisted gas had a lower hardness increase in the other treatment with different number of passes, compared to the experiment with compressed air. Other than the hardness tests, SEM images show that micro cracks were found everywhere in the treated areas of all passes in the experiments with nitrogen gas (Figure 7). In contrast, no micro crack was found in the experiment with compressed air.

Since the material surface did not became solid, in the experiments with nitrogen as assisted gas, the micro cracks might be the main reason that the hardness increase was restricted on the material surface. Therefore, compressed air was chosen as the assisted gas for the following experiments.

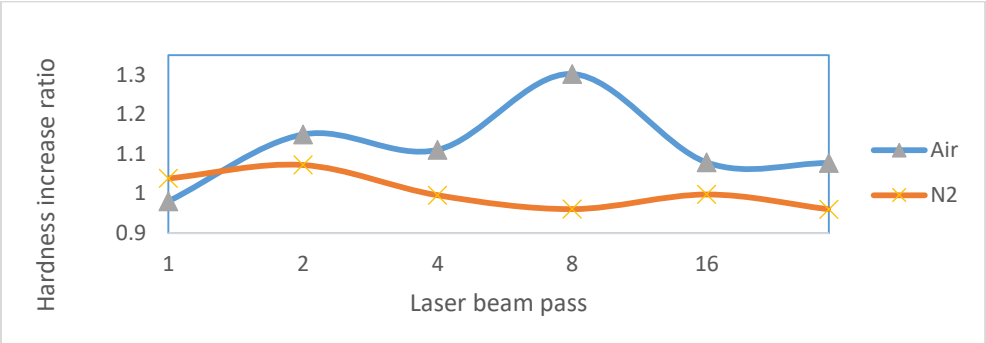

Figure 6: Comparison of compressed air and nitrogen LWH treated results

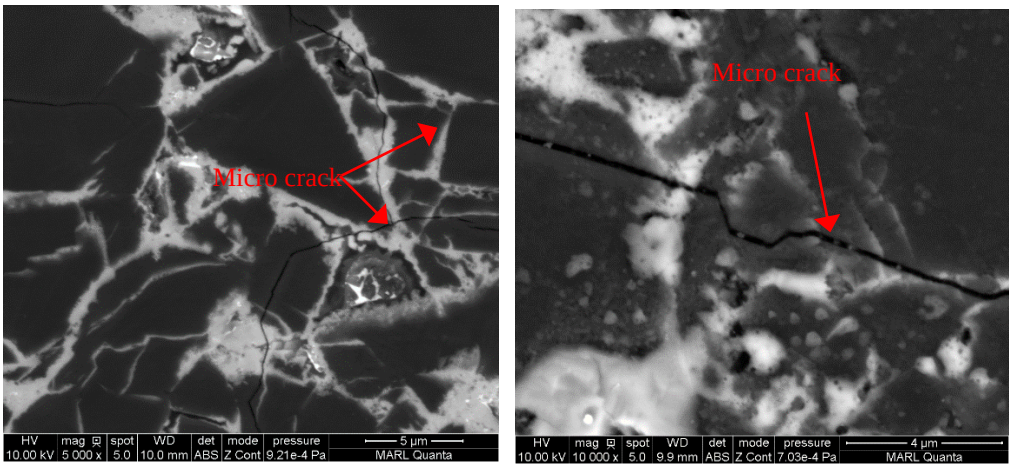

Figure 7: SEM micrograph of LWH treated BN composite

Visual examination of a sample that was laser heat-treated revealed a color change from light-absorbing black/gray to transparent white on the center of the laser beam track (about 200 micron width). Figure 8 shows the color change of the LWH treated area on SEM. Such an effect is ascribed to a change in crystal morphology following S. Veprek's classification of the

crystalline morphology of cBN according to color, size and transparency [25]. A transparent color of white to amber in cBN implies tetrahedral crystal morphology (as opposed to octahedral) with small grain size and loss of boron. It can also be noted that the color may also be caused by inclusions, dopants or defects. The formation of transparent white color of the cBN provides some clues on the possible phase, stoichiometry and grain size changes in laser water-jet heat treatment.

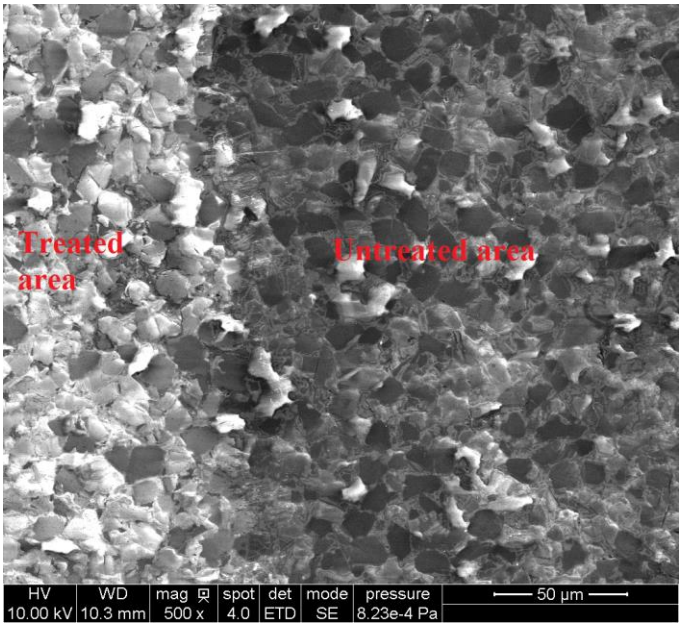

Figure 8: SEM micrograph of cBN showing color change in LWH-treated area

It is noted that the color change occurred only in the center of the laser beam track. The width of the laser beam track was 1 mm, but the width of the color change area was 0.2 mm. This result is attributed to the Gaussian beam laser intensity distribution not being uniform across the laser beam track. According to equation 1, laser beam intensity is higher in the center of the laser beam track than the other areas. Therefore, color and hardness changes were observed to be more intense in the center of the laser beam track.

The hardness was measured from the edge to the center of the laser beam track for each laser pass. Figure 9 shows the SEM images of the indentations taken from the edge to the center of the laser beam track. The 5 laser beam pass areas in one laser beam track were divided by 5 different lines with different distances from the area edge (50, 150, 250, 350, and 450 micrometers from the center of the laser beam track). There are 5 indentations on each line to minimize the inclination.

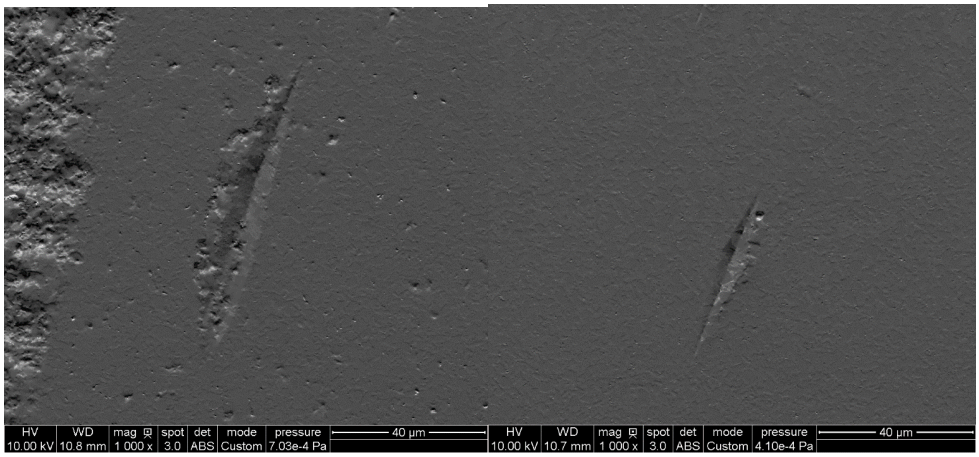

Figure 9:SEM images of the indentations: (left) untreated and (right) LWH treated dual phase cBN/TiN

Figure 10 shows the hardness change ratio results of Knoop hardness tests for bindered 55%cBN/45%TiN as a function of laser beam passes. As shown in Figure 10, the hardness of LWH-treated samples increased by approximately 21% for the indentation placed 150 microns from the center of the laser beam track for 8 laser beam passes. The hardness of treated sample increases about 10% for 1, 2, and 4 laser beam passes, which is not significant compared with 8 laser beam passes area.

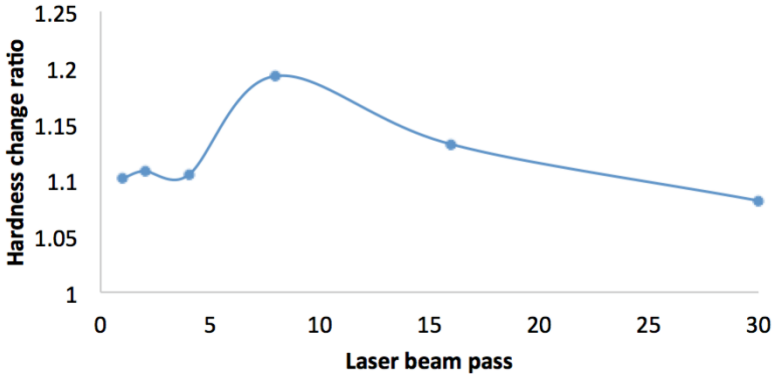

Figure 10: LWH treated 55%cBN/45%TiN material hardness change ratio

Figure 11 shows the hardness change ratio comparison results of Knoop hardness tests for bindered 82%cBN/18%AlN as a function of the laser beam passes. As shown in Figure 11, the hardness of the LWH-treated sample increased by up to 30% for the indentation placed 50 microns from the center of the laser beam track for 8 passes.

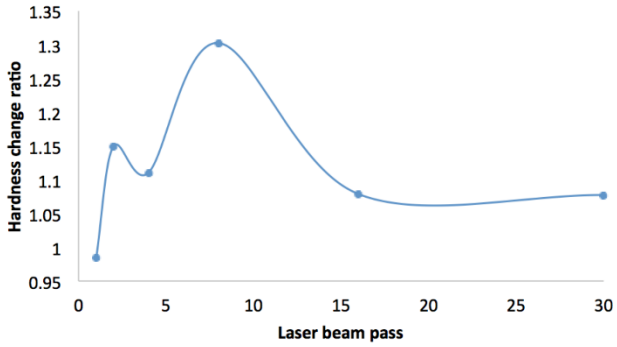

Figure 11: LWH treated 82%cBN/18%TiN material hardness change ratio

Figure 12 shows the hardness change ratio results of Knoop hardness tests for bindered 100% cBN as a function of laser beam passes. As shown in Figure 12, the hardness of LWH-treated sample increased by approximately 20% for the indentation placed 50 microns from the center of the beam track for 30 laser beam passes. The hardness change ratio, which is observed in Figure 12, shows an increased trend with the increase of laser

beam passes. This result matches with our previous study that the hardness of pure cBN was increased up to about 20% on 30 passes and will keep or drop the hardness change ratio with more laser beam pass number over 30.

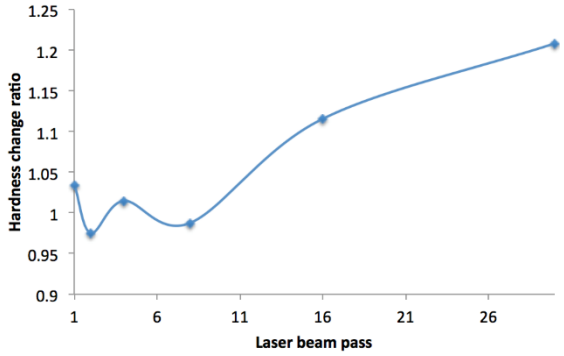

Figure 12: LWH treated pure cBN material hardness change ratio

The hardness change ratio as a function of distance from the laser beam center, shown in Figure 13, was observed as a decrease of hardness change ratio with the increase of distance from the beam center. The hardness of LWH-treated sample increased by approximately 30% for the indentation placed on 50 micrometers from the beam center.

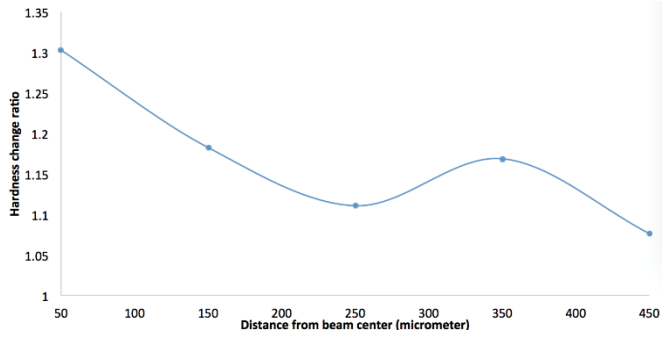

Figure 13: LWH treated pure cBN material hardness change ratio as a function of distance from laser beam center

2.4 Discussions

Results showed a direct correlation between the number of laser beam passes and the hardness for BN composites. It is noticed that the hardness change ratio was more pronounced in the center of the laser beam track as opposed to the edges of the track in most cases. The radial distance, r, of Equation 1, increases as it moves from the center and towards the edges. Thus, the laser energy in the center of the laser beam track is more than that of the track edges resulting in higher temperatures in the center of the laser beam track. The waterjet following the laser beam rapidly quenched the material to room temperature, which created high compressive stresses. The combined action of high temperatures and compressive stresses might have led to microstructure refinement that resulted in the hardness enhancement observed in this study. We believe that as the number of laser beam passes increased, microstructure refinement generated during the LWH process resulted in improved hardness for BN composites. Thus, three points of interest can be taken from this study:

1. The LWH-treated BN composite hardness improved with more laser beam passes;

2. The LWH-treated BN composite hardness increased with decreasing distance from the laser beam center, and the maximum hardness value was observed on the laser beam center.

3. The cBN content in BN composite has a relationship with the LWH treated BN hardness change ratio and the optimal BN content was observed on 82%cBN/18%AlN.

However, these points are not necessarily always valid. According to experimental results, the maximum hardness improvement for the 55%cBN/45%TiN composite occurred after 2 passes in an area located 150 microns from the center of the laser beam track. For the 82%cBN/18%AlN composite, the maximum hardness improvement occurred in the center of the laser beam track after 8 passes, but not the 30 passes, which contributed the maximum

fluence. As the number of passes increases, higher temperature changes can result in higher compressive stresses created by LWH treatment, which may lead to surface damage. Previous studies have reported the presence of spalled regions on LWH-treated cBN/wBN composites [30]. In this study, surface damage was noticed in the center of the laser beam track for 16 and 30 passes on the LWH-treated 82%cBN/18%AlN composite shown in Figure 14. As with the spalled regions identified in our previous experiments, the damaged surface displayed a lower average surface roughness compared to the surrounding areas that did not appear to be damaged. Surface damage can be avoided in future experiments by careful control of the number of laser beam passes admitted on the sample surface.

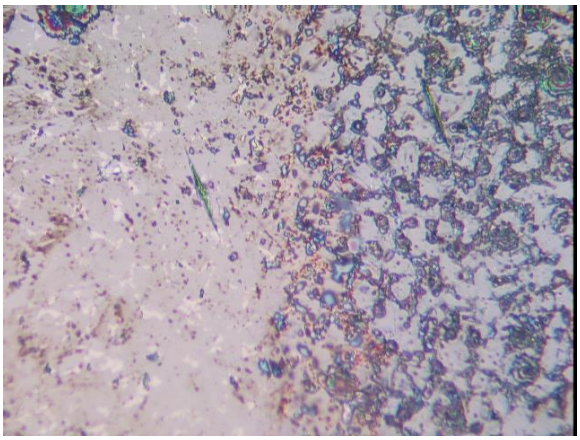

Figure 14: Surface condition of LWH treated 30 passes area of 82%cBN/18%AlN composite

2.4.1 Microstructure of the sample before LWH treatment

Since the hardness increase of the dual phase cBN/TiN and cBN/AlN composites was significant, the reasons for the hardness change were further studied using SEM/EDS to analyze the microstructure and elemental information of the samples. The SEM study revealed images that indicate the formation of significant cracking and fracturing of cBN particles dur-

ing the LWH treatment. The microstructure of the untreated 82%cBN/18%AlN sample consisted of two types of structures with different size and morphology. The first type of structural formation was identified as polyhedral faceting with facets of 1-10 μm in length with dark color shown in Figure 15. The second type of structure observed was identified as irregularly shaped particles (unable to observe the grain boundary) with bright color shown in Figure 15. Polyhedron interfaces have straight-line boundaries with bright material filled in. The polyhedral grains are originally the cubic boron nitride grains, and the bright grains are alumina nitride according to EDS results in Figure 15.

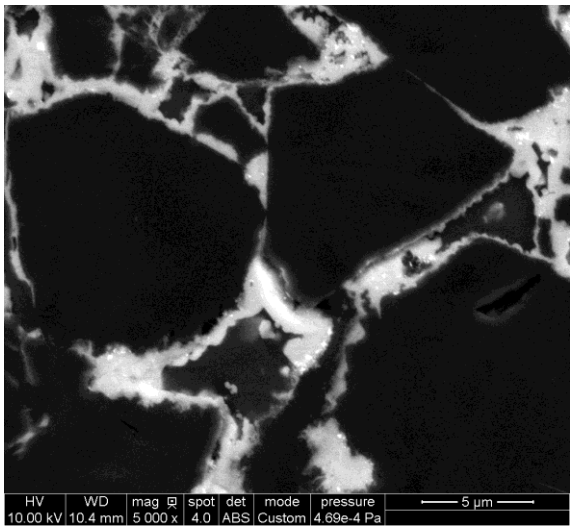

Figure 15: SEM micrograph showing microstructure of untreated 82%cBN/18%AlN sample

Similar to the untreated 82%cBN/18%TiN sample, the dual phase 55%cBN/45%TiN sample consisted of 3 types of particles, which are shown in Figure 16. The first type was identified as trapezoidal particles with dark black color. The second type was identified as grayish particles without a visible grain boundary. The third type of particle was identified as nano-scale

irregularly shaped particles with bright color. EDS results shown in Figure 16 identify the trapezoidal particles as CBN, the gray particles as TiN particles, and the bright particles as a mixture of tungsten, alumina, and nitrogen composite.

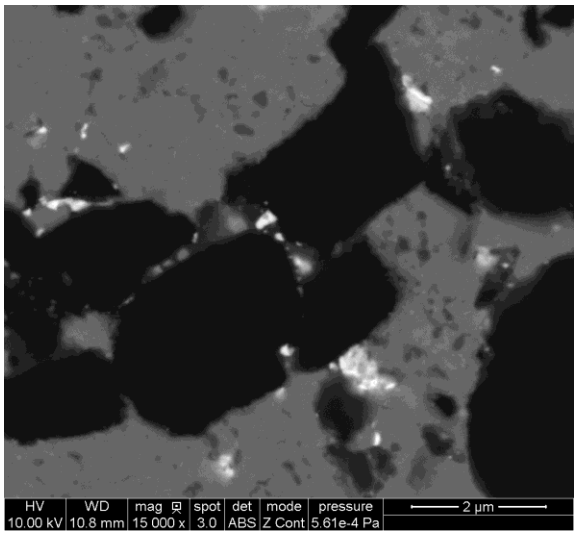

Figure 16: SEM micrograph showing microstructure of untreated 55%cBN/45%TiN sample

2.4.2 Microstructure of the sample after LWH treatment

The microstructure of the cBN/AlN composite after LWH treatment consisted of the same two kinds of grain: the irregular shapes (AlN particles) and the polyhedrons (cBN particles). However, there were two main differences in the observed microstructure for the LWH-treated samples.

There was no dramatic change in the microstructure of the AlN particles because their grain boundary was not visible in the SEM images. However, the first main difference was that the polyhedron particles appeared to be cracked and broken into several smaller particles as shown in Figure 16. According to the EDS point analysis results shown in Figure 19, the gap created by the crack was filled by AlN particles.

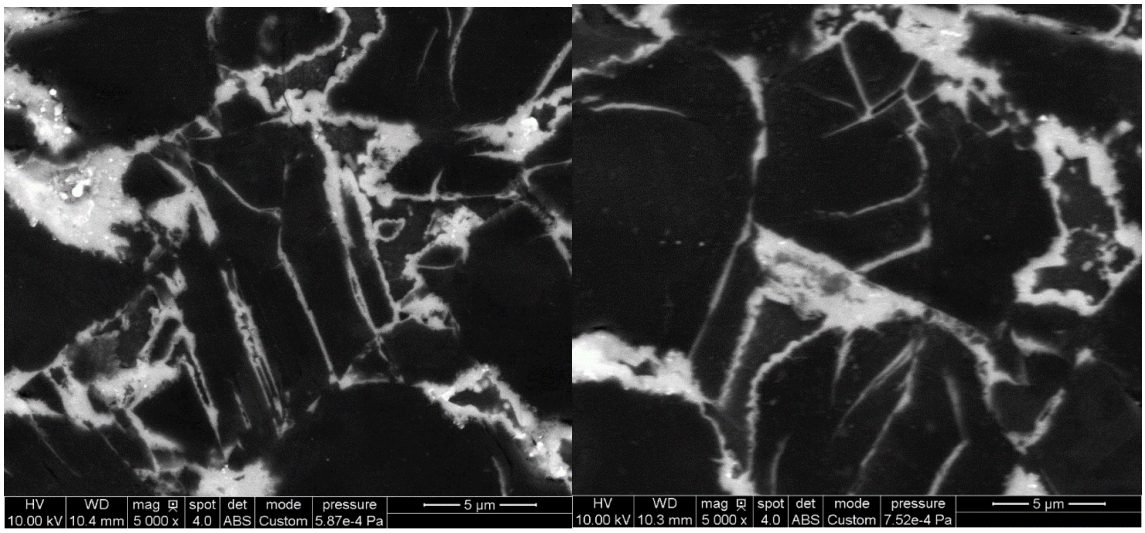

Figure 17: SEM micrograph showing the LWH-treated microstructure of cBN/AlN composite

Since single cBN particles appear to be broken and cracked into several smaller particles, the average particle size in LWH-treated samples was changed. In this paper, the grain size of the samples was calculated by using the standard formula of linear intercepts method:

$$G = 1.56L/MN \tag{4}$$

where G is the grain size, L is the random line length on the micrograph, M is the magnification of the micrograph, and N is the number of the grain boundaries intercepted by the lines [43]. The average grain size of each sample was estimated from two images. For each image, four random lines were drawn to calculate the grain size.

It is commonly accepted that material hardness increases when the grain size decreases which means that the material follows the Hall-Petch effects [44, 45]. However, the grain size of a material is not the only factor that impacts material hardness. Crystallinity, precipitation along the grain boundary, porosity, and slip planes also influence increases and decreases in material hardness [43]. The calculated average grain sizes for this study are listed in Table 2.

Results show an increase in hardness with decreasing grain size among the different samples. The average grain size of LWH-treated cBN/AlN composite decreased from 5.644 μm to 3.026 μm, which was 46.4% less than the untreated sample. The hardness of LWH-treated cBN/AlN composite increased from 46 GPa to 60 GPa, a 30% increase compared to untreated cBN/AlN composite. This hardness and grain size change is consistent with Hall-Petch effects.

Table 4: Calculated grain size of BN composites

Material	**55%cBN/45%TiN**		**82%cBN/18%AlN**	
	untreated	**LWH treated**	**un-treated**	**LWH treated**
Average grain size (μm)	0.553	0.237	5.644	3.026
Change ratio		0.428		0.536

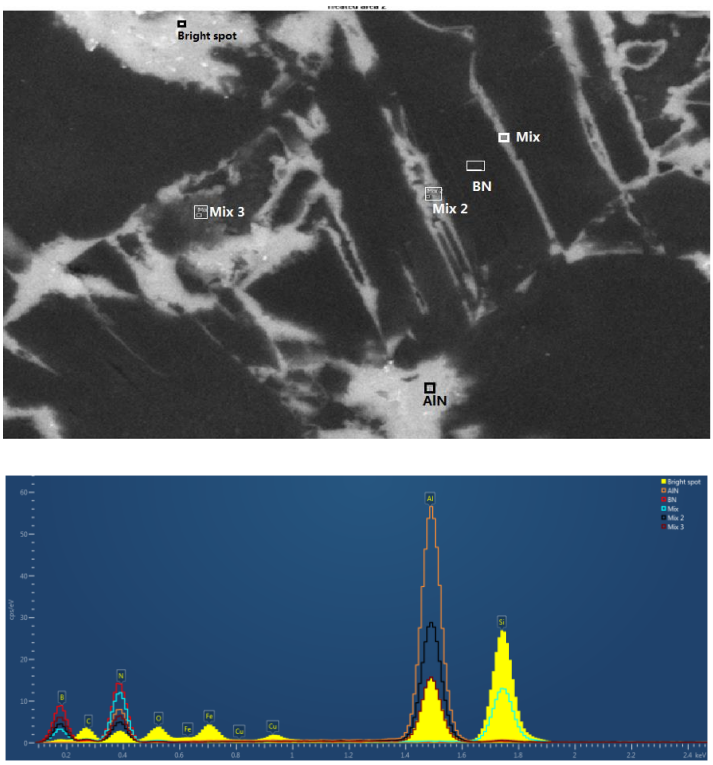

Figure 18: SEM point analysis of LWH treated cBN/AlN composite

Several mechanisms were attributed to the hardness increase of cBN/TiN composite. First, the formation of nano-scale cBN grains not detected in untreated cBN/TiN composite can be seen in LWH-treated cBN/TiN composite shown in Figure 18. The nano-scale structure of the cBN grains is expected to introduce a grain-boundary strengthening mechanism which inhibits ease of dislocation movement across the boundary [46]. The second observed mechanism attributed to increased hardness of cBN/TiN composite was the change in grain size of the composite after LWH treatment. Similar to LWH-treated cBN/AlN composite, the average grain size of cBN/TiN composite was decreased from 0.553 µm to 0.237 µm which is 57.2% less than the average grain size of the untreated sample. This kind of structure change is expected to increase the energy needed to allow for dislocations among grains.

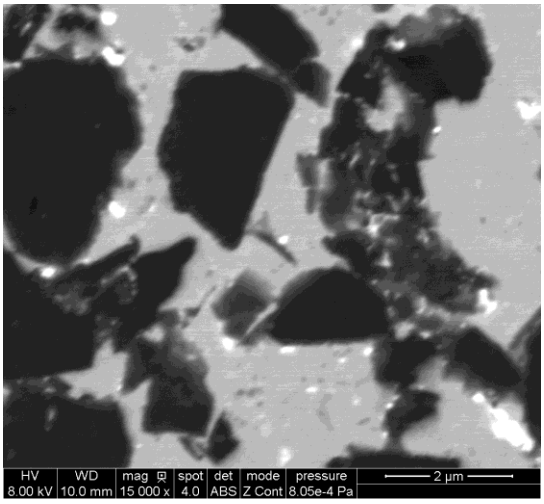

Figure 19: SEM image of LWH treated cBN/TiN composite

It is interesting to note the breaking of cBN particles to several smaller particles and the transition of filler materials to close the gaps between the newly developed smaller cBN particles. According to EDS results, the filler materials were identified as tungsten, alumina, and titanium. Tungsten and alumina were impurities while titanium nitride was a main particle in the composite.

It can be concluded that grain-boundary strengthening due to formation of cracks of large CBN particles and significant reduction in grain-size of the material are the dominant mechanisms of hardness improvement for BN composites

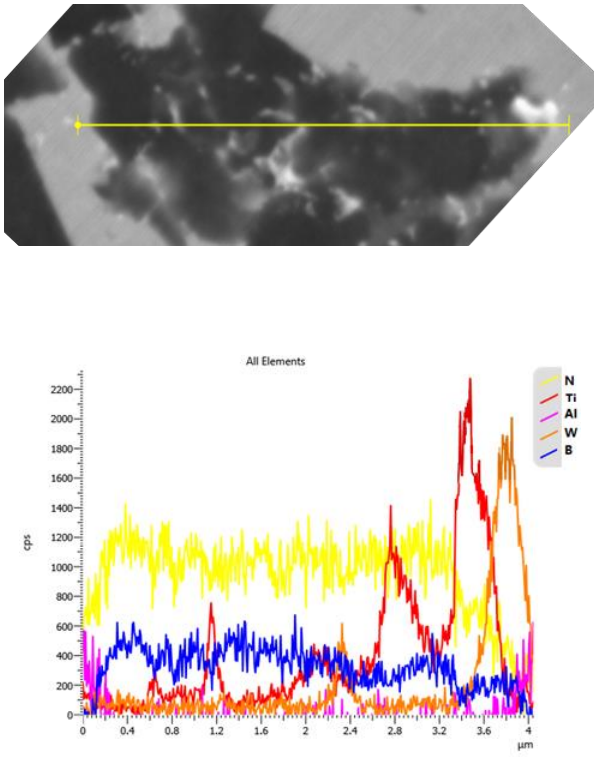

Figure 20: EDS line analysis of LWH treated cBN/TiN composite

2.5 Conclusions

Laser waterjet heat treatment experiments with nitrogen as the assisted gas showed that the hardness of both materials increased after the heat treatment under the suitable laser parameters. However, it is noted that the experiments with nitrogen gas did not contribute a higher hardness increase in the microhardness test, compared to the experiment with compressed air. In the experiments with nitrogen as assisted gas, the lower hardness increase attributed to micro cracks. Thus, the compressed air was chosen as the assistant gas for the following experiments.

In the experiment with compressed air, the hardness of LWH treated pure cBN (100%cBN) increased up to 23%, the hardness of commercial BN composites (82%cBN/18%AlN) with

high contents of cBN increased up to 30%, and the hardness of 55%cBN/45%TiN composites increased up to 21%. Commercial BN composite, though less pronounced on the effect of heat treatment, displayed similar hardness change mechanisms that helped in understanding why hardness improved after LWH treatment. In addition, this paper observed that there is a relationship between BN composite hardness change ratio and cBN composition. In order to maximize the BN composite hardness, a series of experiments will be designed and conducted to investigate this kind of relationship in the future.

The composite microstructures examined by SEM indicated that the formation of zones with nano-sized grains lead to the grain-boundary strengthening mechanism. A significant grain size change after LWH treatment was also detected in this study. These kinds of microstructure and grain size changes are expected to increase the energy needed to move dislocations that increase the hardness of the composites. Future hardness improvement studies of cBN/wBN composites could include the development of a mathematical model that can be used to optimize the combined effects of cBN and wBN with respects to composition, microstructure, grain size, and the binder phase of cBN/wBN composites.

Acknowledgment

The authors would like to gratefully acknowledge the financial support provided by Tianjin University of Science and Technology, China under the Grant 2016LG22. The authors would also like to thank Dr. Volodymyr Bushlya and Dr. S. Lehmann from Lund University, Sweden for providing the Boron Nitride samples.

CHAPTER 3: HARDNESS CHANGE DURING WATER ASSISTED PULSED LASER HEAT TREATMENT OF POLYCRYSTALLINE CUBIC BORON NITRIED TOOL MATERIALS

A paper prepared for publication in *the journal of Advanced Manufacturing Technology* (2017)

Kwang Shiong Wong[1,2], Pranav Shrotriya [1,3]

Abstract

For decades, cubic boron nitride (cBN) material has been widely utilized for cutting tools because of its high hardness, chemical stability and thermally stability. Even though the hardness of cBN is much lower than diamond, the increase in hardness of cBN is still an interesting topic. In this study, a water assisted laser heat treatment was introduced to increase the hardness of cBN without damaging the surface of the sample. The change in hardness was investigated using Knoop hardness measurement and the microstructures of the material surfaces were characterized using Scanning Electron Microscope (SEM). Two sets of experiments were conducted, which were the treatment of multiple passes on a single line and the treatment of a 2x2 area.

[1] Department of Mechical Engineering, Iowa State University, Ames, IS 50011, USA
[2] Primary researcher and lead author
[3] Co-author

3.1 Introduction

Continuous wave (CW) and pulsed lasers are the most commonly used lasers in industry and research. CW laser means the laser continuously emits beam light at a certain frequency[9]. On the other hand, pulsed laser depends on the repetition rate, pulse duration, and peak power. The laser with a shorter pulse width produces a higher peak power. For example, a nanosecond laser produces a peak power up to gigawatts and a femtosecond laser produces a peak power up to petawatts. An advantage from the pulsed laser over CW laser is that pulsed laser creates a small heat-affected zone to the material due to it short pulse width, whereas CW laser creates a large heat-affected zone because the heat of the laser beam transfers throughout the entire material. Pulsed lasers are commonly used in micromachining, cutting, and deposition.

Hardness is defined as “resistance of metal to plastic deformation” [1] and caused cutting, abrasive, and scratching. According to Heath, only diamond and cubic boron nitride can be considered as ultrahard materials because their Vickers hardness is greater than 35 GPa [3]. Diamond is the hardest material on earth and can be found in nature. However, diamond is not an ideal material used for cutting ferrous materials because of its thermal instability. At a cutting temperature of 650 C, diamond reacts with ferrous materials to form iron carbide. On the other hand, cubic boron nitride (cBN), the hardest man-made material but less so than diamond, is still stable in air and vacuum and does not react with any material at the temperature of 1550 C. Although cBN is more stable at a high temperature, it still cannot substitute diamond because its hardness is much lower. Therefore, the recent research has focused on improving the hardness of their materials in order to reach the hardness of diamond.

The Hall-Petch effects explain that the increase in hardness is related to the grain size

of the material. A decrease in crystalline size caused an increase in hardness due to the dislocation activity in grains [44]. If the grain size is smaller, more energy is required to dislocate the grains, so the hardness of the material increases.

Kalyanasundaram proposed a method to effectively break the large particle into small particles. His analytical model and experimental results were the same: the laser waterjet (LWJ) process resulted in the thermal shock-assisted fracturing of particles into microstructure refinement, compared to melting, vaporizing, and solidifying the material surface. In LWJ, a temperature gradient was created in the laser heating and the quenching effect created thermal stresses that fracture the large particles into small particles [47].

Some similar works have done By using the laser water jet process with CO_2 continuous wave laser, Melaibari applied multiple overlapping passes with an overlap of 50% from the sample of cBN/wBN composites and received about 90% hardness increase in this sample[48]. By using the sample laser system, Zhao applied multiple passes of laser beam over the same location and investigated to the change of hardness and mircosctruture. Zhao obtained a 50% hardness increase on cBN/wBN composites without damaging the sample surface from the LWJ heat treatment [49]. They proved that the quenching effect play an important role in the change of hardness in the laser surface treatment.

This paper will describe the results of an experiment examining the change in hardness of cBN. By using a pulsed laser and varying the number of laser beam passes and the condition of quenching effect, the mechanism of the increase in hardness of cBN was investigated.

3.2 Experimental detail

3.2.1 Laser system setup and dual-phase materials

A nanosecond pulsed Nd:YAG laser system (Quanta-Ray INDI-30), capable of producing a pulse of 1-10 Hz repetition rate, 7 ns pulse width, a wavelength of 532 nm, a maximum average power of 0.4 W and a peak power of 2e7 W, was used to conduct heat surface treatment. The Q-switch mode was selected so the repetition rate could be adjusted. The power and repetition rate of the laser were monitored using a local controller. The laser beam was reflected using a mirror and focused using a high energy focused lens with a working distance of 35 mm. A 2D motorized stage was applied to control the laser motion and the stage was monitored by a computer. Two types of commercial samples of cBN were used in this study: dual phase (1) 82%cBN/18%AlN and (2) 55%cBN/45%TiN. Before the experiments, the average hardnesses were reported 34.94 GPa for 82%cBN/18%AlN and 24.31 GPa for 55%cBN/45%Ti. Before the heat treatment, the sample surface had to be polished into a reflective surface, otherwise the oxidation layer and defects would prevent the visibility of indentations. The polishing steps were 15 um, 9 um and 1 um diamond suspensions.

3.2.2 Laser surface treatment

In this work, average powers of 0.03 W and 0.015 W were applied to the sample of 82%cBN/18%AlN and 55%cBN/45%TiN, respectively, with a repetition rate of 4 Hz. The sample was placed on the stages and the distance between the focused lens and the top surface of the sample was 40 mm in order to defocus the laser beam to a spot size of 1.27e-4 um. Two sets of experiments were done for each material. In the first set of experiment, five levels of laser beam passes, which included 1 pass, 2 passes, 4 passes, 8 passes and 16 passes, were

investigated and the hardness tests were done after these treatments. Under each laser beam pass, a 1 mm line was treated. In the second set of experiment, the number of passes that contributed the greatest hardness increase in the first experiment was chosen to treat an area of 2 mm x 2 mm for both samples. For each experiment, the samples were submerged into water with 1 mm of water was covering the top surface of each. The water could quench the materials to room temperature. Besides the water treatment, the experiment was also done without water for both samples in order to investigate the quenching effect.

3.2.3 Measurement of micro-hardness

The indentation hardness tests were done by using a Tukon micro-hardness tester with a pyramid-shaped Knoop diamond indenter. A 5 N load was applied on each indentation and the duration was set to 30 s. Fifteen indentations were made on untreated and heat-treated areas to ensure the reliability of the test data. The images of each indentation were taken by a high-resolution optical microscope. Hardness measurements were made on the length of the horizontal axis of the indentations in a Java-based image processing program known as ImageJ to ensure the accuracy of the measurements. The indentations were also made on the outside area of the laser beam track to investigate the heat transfer made by the nanosecond laser.

3.2.4 Investigation of micro-structure and phase composition

Scanning Electron Microscopy (SEM) was performed on HRSEM LEO/Zeiss 1560 in high current mode to investigate the micro-structure of the samples before and after the heat treatment for both samples. Due to the problem of sample charging, a thin layer of Iridium was coated on each sample surface.

3.3 Experimental results

3.3.1 Visual examination

The laser treatment caused a significant color change to the surfaces of both samples. By eye observation, treated areas of both samples had a darker color than the untreated area, shown in the Figure 20. It was noted that the color change was found only in the center of the laser beam track. However, the area outside of the laser beam track remained the same color as the untreated area.

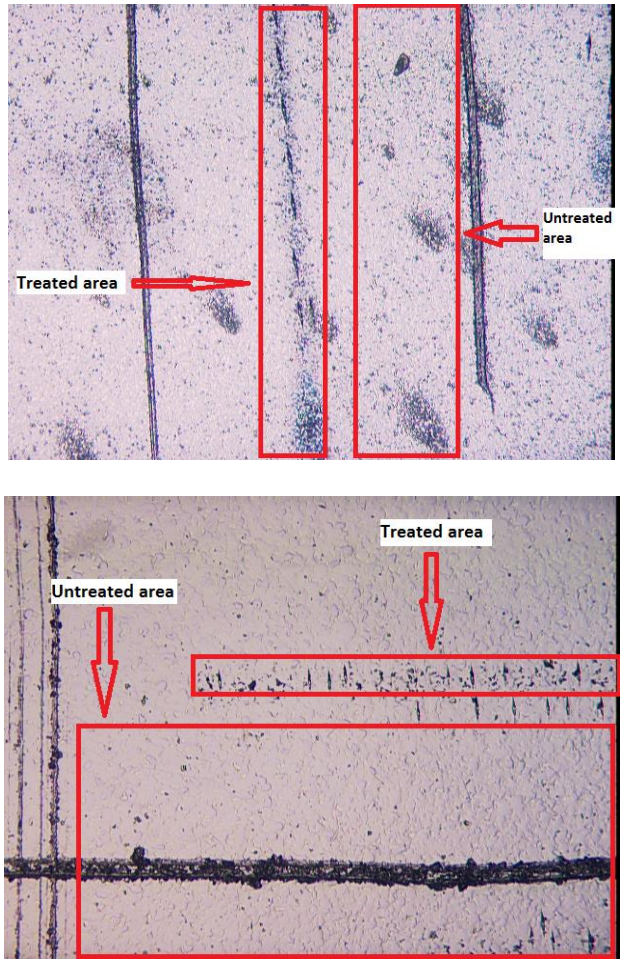

Figure 21: Comparison between untreated area and treated area (top:82% cBN, bottom:55% cBN)

3.3.2 Micro-hardness test

In the first set of experiments, results of the hardness tests on the untreated and treated areas with and without water were shown in Table 5 and 6. In the heat treatment with water, the highest hardness increase ratio up to 20% with a result of 42 ± 3 GPa was found in the sample of bindered 82%cBN/18%AlN in the 8-pass level. In addition, the highest hardness increase ratio up to 18% with a result of 34 ± 2 GPa was found in the sample of bindered 55%cBN/45%Ti in 4-pass level. However, the hardness increase happened only on the laser beam track. The hardness outside of the laser beam track remained the same as the untreated area. Besides the experiment with water, the hardness increase of the experiment without water treatment was not obvious, contributing only about 8% in the sample of bindered 82%cBN/18%AlN and -2% to 4% to the sample of bindered 55%cBN/45%Ti.

Table 5: 82% cBN heat treatment with and w/o water

	With water			***Without water***		
Number of passes	Average hardness (GPa)	Increase ratio (%)	Standard deviation (GPa)	Average hardness (GPa)	Increase ratio (%)	Standard deviation (GPa)
0	34.94	-	-	34.94	-	-
1	39.07	6.01	3.57	37.57	7.53	5.35
2	37.61	7.65	3.53	37.63	7.70	2.75
4	41.01	17.37	2.62	38.00	8.77	4.75
8	42.08	20.42	3.55	37.97	8.66	4.88
16	41.82	14.18	3.6	37.80	8.18	4.22

Table 6: cBN heat treatment with and w/o water

	With water			***Without water***		
Number of passes	Average hardness (GPa)	Increase ratio (%)	Standard deviation (GPa)	Average hardness (GPa)	Increase ratio (%)	Standard deviation (GPa)
0	24.31	-	-	24.31	-	-
1	28.02	15.24	1.92	25.38	4.38	3.02
2	28.12	15.66	2.12	23.96	-1.46	1.18
4	28.78	18.39	1.71	25.80	6.10	2.90
8	25.44	4.63	1.68	25.34	4.23	3.32
16	26.76	6.43	2.42	23.78	-2.20	1.42

One number of passes was chosen for both samples for the second set of experiments based on its overall performance. 8-pass level performed the best in hardness increase for the sample of bindered 82%cBN/18%AlN, but the worst for the sample of bindered 55%cBN/45%Ti. Furthermore, the hardness increase of 4-pass level was close to 8-pass level in the sample of bindered 82%cBN/18%AlN, and it performed the best in the sample of bindered 55%cBN/45%Ti.

In the second set of experiments, 4-pass level was chosen to treat an area of 2 mm x 2 mm for both samples and the samples were submerged into water, since this level of pass number contributed the best performance in the first set of experiments. The results of both sample after heat treatment was shown in Table 7.

Table 7: Hardness increase ratio of 2x2 area

Sample	Hardness increase ratio (%)
82%cBN	14.65
55%cBN	15.99

3.4 Discussion

It was reported that the hardness increase and the color change of the sample surface were significant in the center of the laser beam track. Since Nd:YAG laser generates Gaussian beam, the laser intensity reached the highest value in the center of the laser beam track and decreased from the center to the outside area.

The number of laser beam passes influenced the material surface. If low-level laser beam passes were applied on the material surface, the fluence became low, resulting in a less helpful heat treatment effect. On the other hand, the higher level laser beam passes contributed more fluence to the material surface. For example, the 1-pass level showed almost no color change for both samples due to the fact that the laser fluence was not high enough. After 1-pass level, some ambiguous treated marks could be seen in the 2-pass level and the color change became more apparent in the higher level laser beam passes.

In the sample of bindered 55%cBN/45%Ti, the hardness increase ratio reached the maximum at the 4-pass level. However, after the 4-pass level, the hardness increase was insignificant at the 8-pass and 16-pass levels. It was noted that the damage threshold of the bindered 55%cBN/45%TiN happened at the 4-pass level. On the other hand, in the sample of the bindered 82%cBN/18%AlN, the 8-pass level was found to be the best. The hardness

increase of the 1-pass and 2-pass levels were not significant because the fluence was not high enough to conduct an effective heat treatment.

Some testing without submerging the samples into the water was also done. Compared to the heat treatment with water, the hardness increase for both samples was insignificant and some hardness decrease was found in the sample of bindered 55%cBN/45%Ti. After the laser beam hit on the material surface, the water rapidly quenched the material to room temperature, resulting in compressive stress. Other than the quenching effect, the hardness at the outside area of the laser beam track was also found to be the same as the untreated area. Since the laser beam was in nanoseconds, the heat was not able to transfer out of the laser beam track, resulting in a small heat-affected zone.

Some SEM images were taken in order to investigate the micro-structure. The formation of cracking and fracturing of particles were found on the treated areas for both samples. The bindered 82%cBN/18%AlN sample consisted of two types of structures with different size and morphology. The dark color particles, which were in polyhedral faceting, were cBN particles, meanwhile the bright color portion, which had an irregular shape, were Aluminum Nitride. In Figure 21, SEM showed that all the cBN particles were complete and not many cracks could be found. Figure 22 showed the microstructure of the sample of bindered 82%cBN/18%AlN after the heat treatment. Single big particles broke into some small particles and the grain size of cBN particles became smaller.

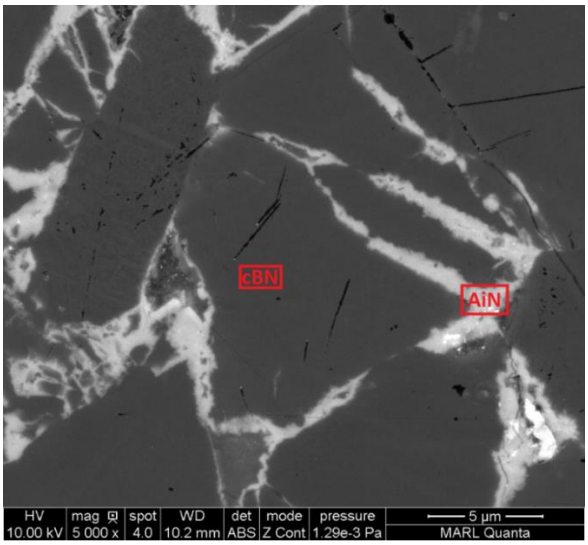

Figure 22: SEM images showing microstructure of untreated 82% cBN area.

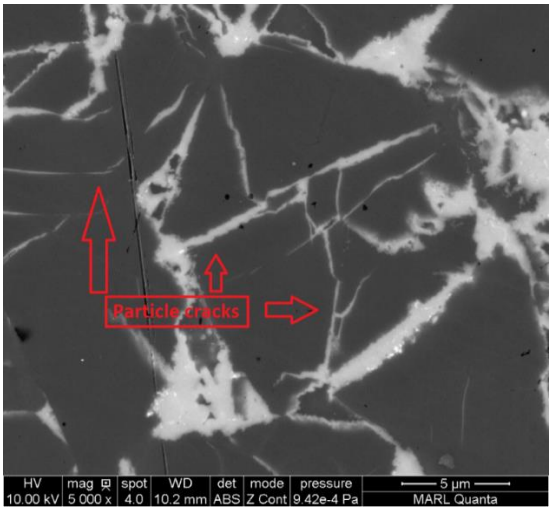

Figure 23: SEM images showing microstructure of 82% cBN after laser heat treatment: 8 passes

However, in the sample of bindered 82%cBN/18%AlN, the increase in hardness in the 16-pass level was lower than the 8-pass level, even though a higher fluence was applied in the 16-pass level. Figure 23 showed the microstructure of the 16-pass. Compared to the image of

the 8-pass level, damages were found in the microstructure of the matrix, which was aluminum nitride. These damages limited the increase in hardness.

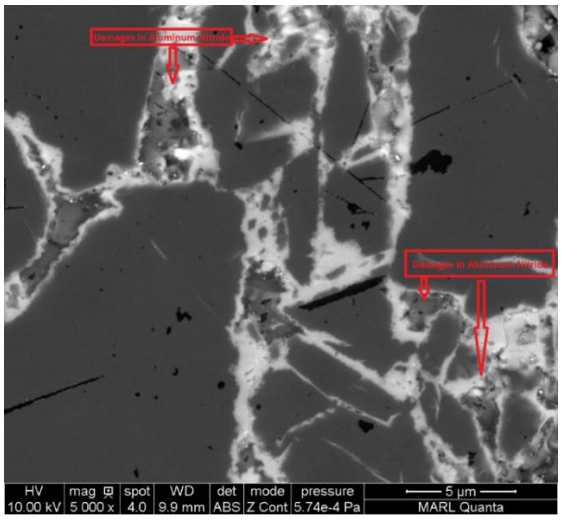

Figure 24: SEM images showing microstructure of 82% cBN after laser heat treatment: 16 passes

Similar to the sample of bindered 82%cBN/18%AlN, the dual phase sample of bindered 55%cBN/45%Ti consisted of three types of particles. Shown in Figure 4, the first type of particles was cBN, which was in dark color. The second type of particle was titanium nitride, which was identified as grayish particle without a visible boundary. The third type particle was a mixture of tungsten, alumina, and nitrogen composites. Figure 24 shows the microstructure of the untreated area of the sample of bindered 55%cBN/45%Ti. All the cBN particle are whole and not many cracks can be found. In contrast, figure 25 shows the microstructure after the heat treatment: a big cBN particle, located in the center, broke into different parts.

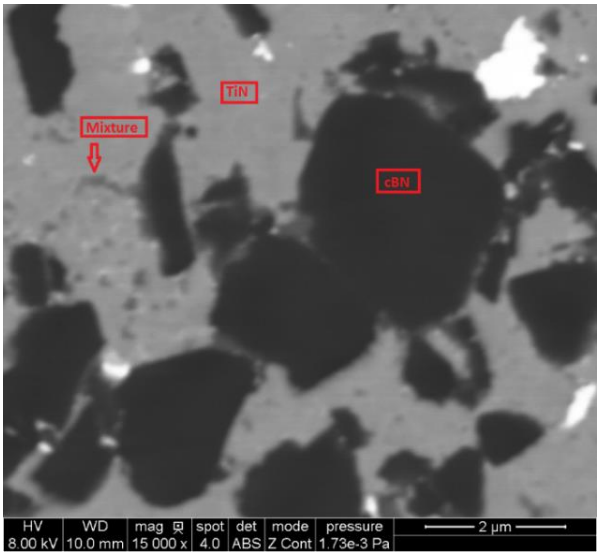

Figure 25: SEM images showing microstructure of untreated 55% cBN area

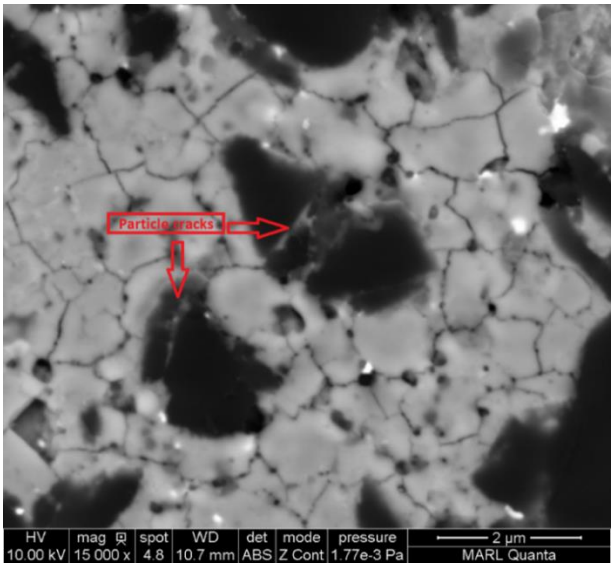

Figure 26: SEM images showing microstructure of 55% cBN after laser heat treatment: 4 passes

Even though the 4-pass level contributed the highest increase in hardness, which was 18%, some damages were also found in this level. On the other hand, in the 8-pass and 16-pass levels, the hardness increase were found to be insignificant, which were 5% and 6%. The damages to the AIN could be found everywhere in the microstructure in these two levels. Figure 26 showed the microstructure of the 16-pass level. The insignificant hardness increase might attribute to the damaged matrix, which were the TiN and the mixture composite. Since the matrix was damaged in the heat treatment and the sample became not solid.

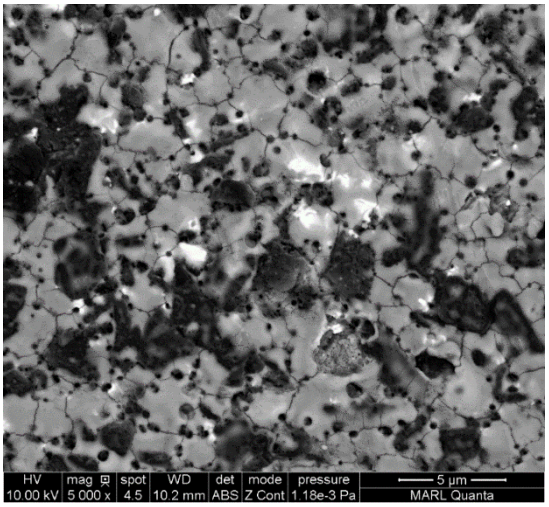

Figure 27: SEM images showing microstructure of 55% cBN after laser heat treatment: 16 passes

According to Hall-Petch effects, when grain size decreases, the hardness of the material increases after treatment [44]. In Figure 27, under the magnification of 500x, an untreated and a treated area of 1x10 units were selected in the SEM image of each pass level to determine the numbers of particles in the untreated and treated areas by using ImageJ. The grain size numbers and average grain diameters were calculated by using the standard formula of ASTM Committee E-4 and Grain Size Measurements[48, 50], which are shown in equation 3 and 4.

$$N = 2^{n-1} \tag{4}$$

$$d = \frac{\frac{25.4^2}{2^{n-1}}}{100^2} \text{ x } 1000 \tag{5}$$

N is the number of grains per square millimeter, *n* is the grain size number and *d* is the average grain size diameter in micrometer. ASTM grain size number increases with decreasing grain size. The grain size numbers for each untreated and treat area were shown in Table 8 and 9. Compared to the untreated areas that are beside the treated areas, the treated areas had more particles and the average diameters of the particles were smaller. Therefore, it could be explained that the hardness increased with decreasing grain size and increasing numbers of particles after the laser heat treatment.

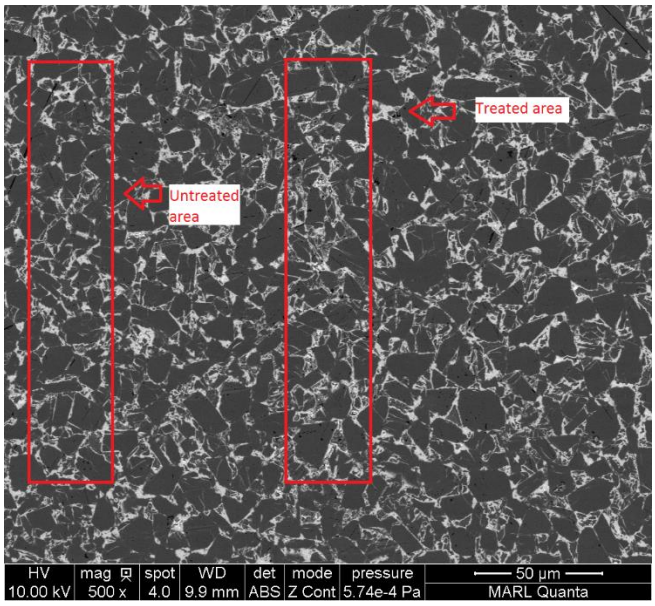

Figure 28: Untreated and treated areas selected for grain size analysis

Table 8: Grain size of 82% cBN

	Untreated area			Treated area			
Number of passes	*N*	*n*	*d*	*N*	*n*	*d*	*Particles increase ratio (%)*
1	43	6.43	0.39	47	6.55	0.37	9.30
2	37	6.21	0.42	51	6.67	0.36	37.83
4	32	6.00	0.45	48	6.58	0.37	50.00
8	48	6.58	0.37	85	7.41	0.28	77.10
16	40	6.32	0.40	73	7.19	0.30	82.50

Table 9: Grain size of 55% cBN

	Untreated area			Treated area			
Number of passes	*N*	*n*	*d*	*N*	*n*	*d*	*Particles increase ratio (%)*
1	229	8.84	0.17	239	8.9	0.16	4.37
2	259	9.02	0.16	279	9.12	0.15	7.72
4	227	8.83	0.17	257	9.01	0.16	13.21
8	224.5	8.81	0.17	352	9.46	0.14	43.96
16	249.5	8.96	0.16	454	9.83	0.12	81.96

Figure 28 and 29 showed the relationship between hardness increase ratio and numbers of particles increase ratio of the bindered 82%cBN/18%AlN and bindered 55%cBN/45%Ti samples, respectively. According to Hall-Petch effect, other than grain size of the material, the change of crystallinity, precipitation along the grain boundary, porosity, and slip planes also

significantly affect material hardness [44]. In the sample of bindered 82%cBN/18%AlN, even though the 16-pass level had more particles than the 8-pass level, it had a lower hardness increase due to the damaged in the matrix. On the other hand, in the sample of bindered 55%cBN/45%Ti, the 4-pass level contributed a better fluence to the material surface, compared to the 8-pass and 16-pass levels.

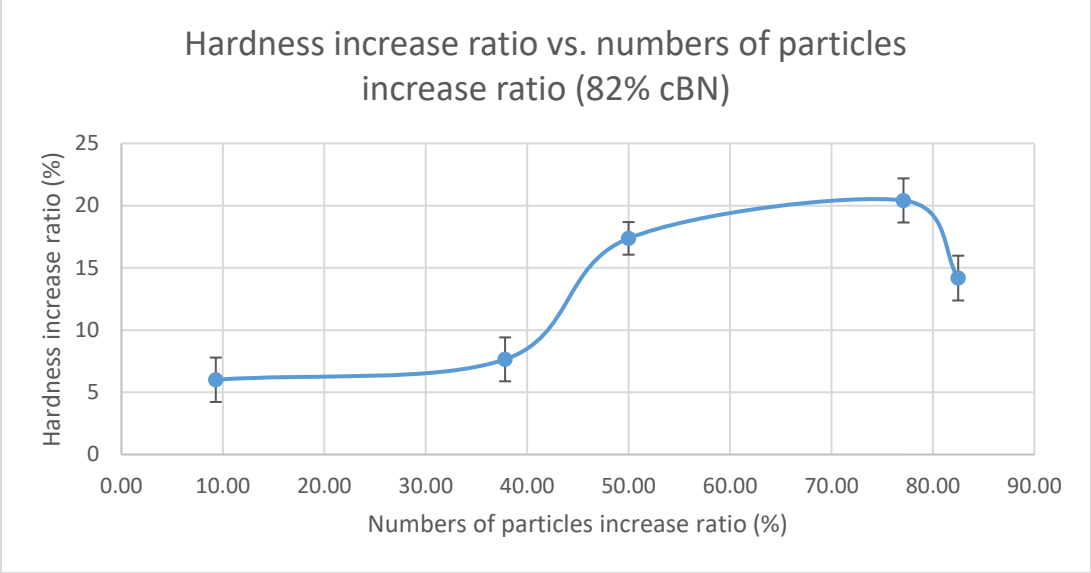

Figure 29: Hardness increase ratio vs. numbers of particles increase ratio (82% cBN)

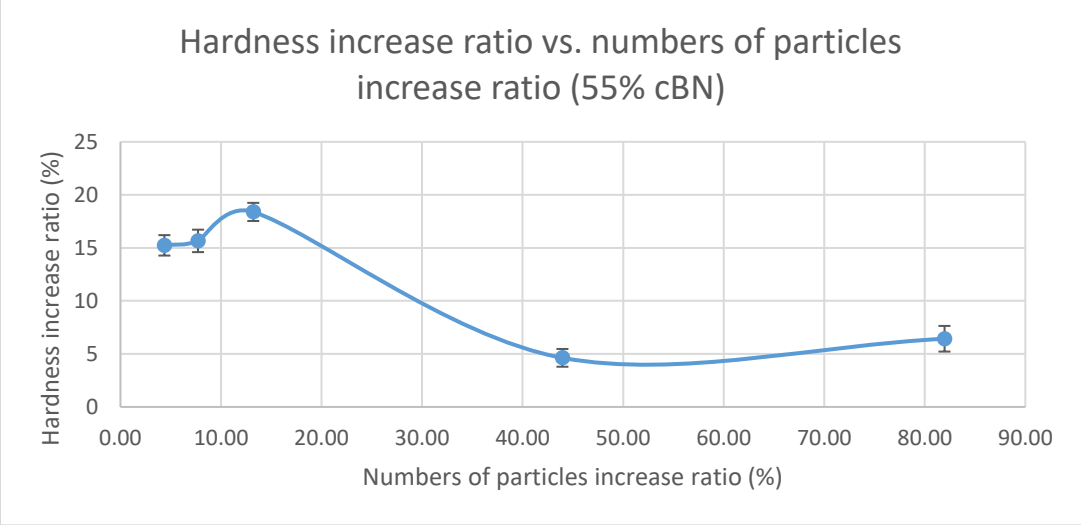

Figure 30: Hardness increase ratio vs. numbers of particles increase ratio (55% cBN)

The following equation shows the Hall-Petch relationship[24]:

$$H = H_o + \frac{K}{\sqrt{d}}$$

H: the hardness of the materials after the laser heat treatment

H_o: the hardness of the materials before the laser heat treatment

K: the strengthening coefficient and

d: is the average grain diameter

The average grain diameter is inversely proportional to the hardness change. The high laser fluence leads to break the grain. If the average grain diameter is smaller, the hardness change becomes more significant. On the other hand, the low laser fluence does not make a significant change to the size and shape of the cBN grains. If the average grain diameter of cBN remains the same, the change of cBN hardness after the heat treatment remains the same as well. Figure 31 showed the relationship between hardness change and diameter change. The blue trend showed the relationship between hardness change and diameter change of the sample of bindered 82%cBN/18%AlN. Due to the high laser fluence, this trend increases from the 1-pass to 8-pass level and starts to go down in the 16-pass level. On the other hand, the red trend showed the relationship between hardness change and diameter change of the sample of bindered 55%cBN/45%Ti. This trend starts to go down in the 8-pass level because the matrix was being damaged by the high laser fluence. In conclusion, from Figure 31, the laser fluence starts to damage the cBN surface at a certain level.

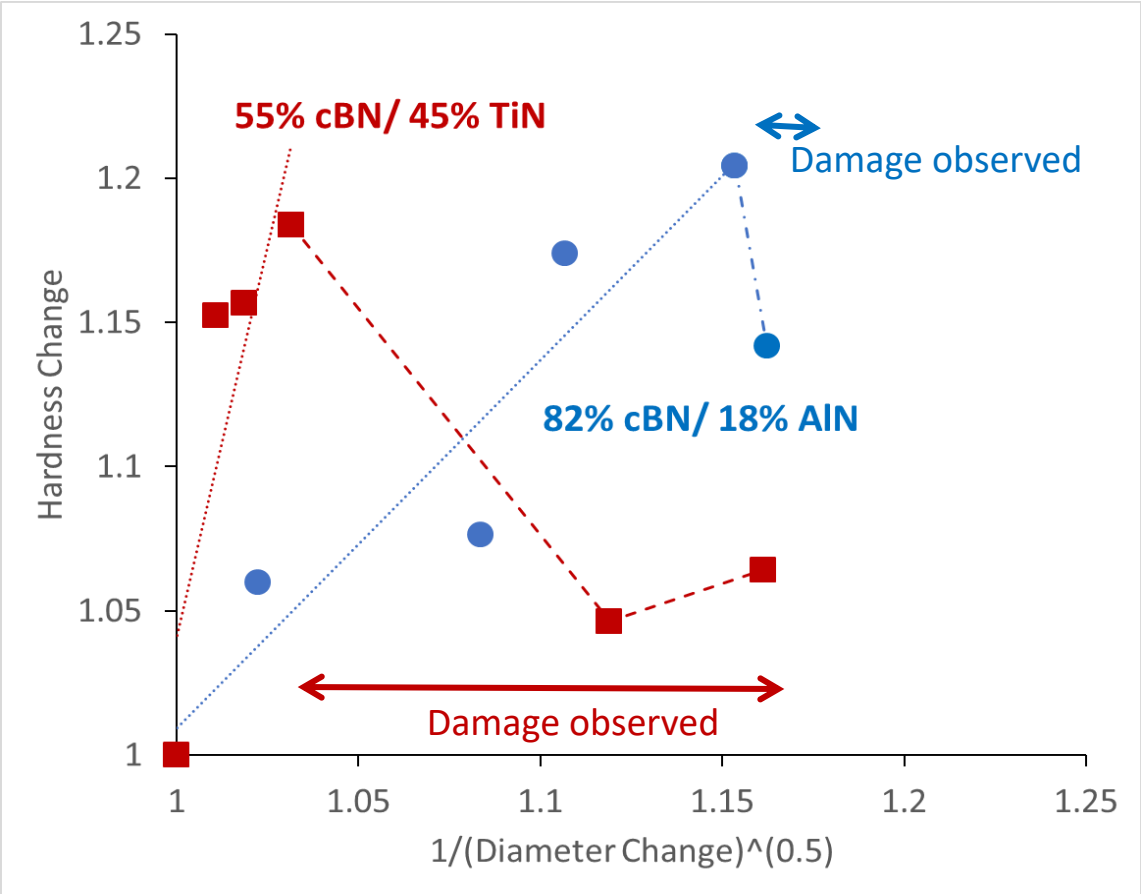

Figure 31: The relationship between hardness change and diameter change in Hall-Petch relationship

In the second set of experiments, the 4-pass level was chosen to treat an area of 2x2 mm. Compared to the first experiments, a lower hardness was found on the 2x2 mm treated area of both sample, Based on the parameters, such as feed rate, repetition rate, and focal length, the actual laser beam spot was designed to have no gap and no overlap for each laser shot. However, the area of the heat-affected zone of each beam spot is unknown, and it would definitely be larger than the area of actual beam spot. This means that the heat-affected zone extends beyond the beam spot for an unknown area. In the single line experiments, the heat-

affected zone overlapped each laser spot only in horizontal. Furthermore, in the 2x2 mm treated area, the heat-affected zone also overlapped each laser spot in vertical. Therefore, in the 4-pass level, the fluence of 2x2 mm treated area was higher than the fluence of single line. Shown in Figure 30, the treated areas of both samples were darker in color, compared to the untreated areas.

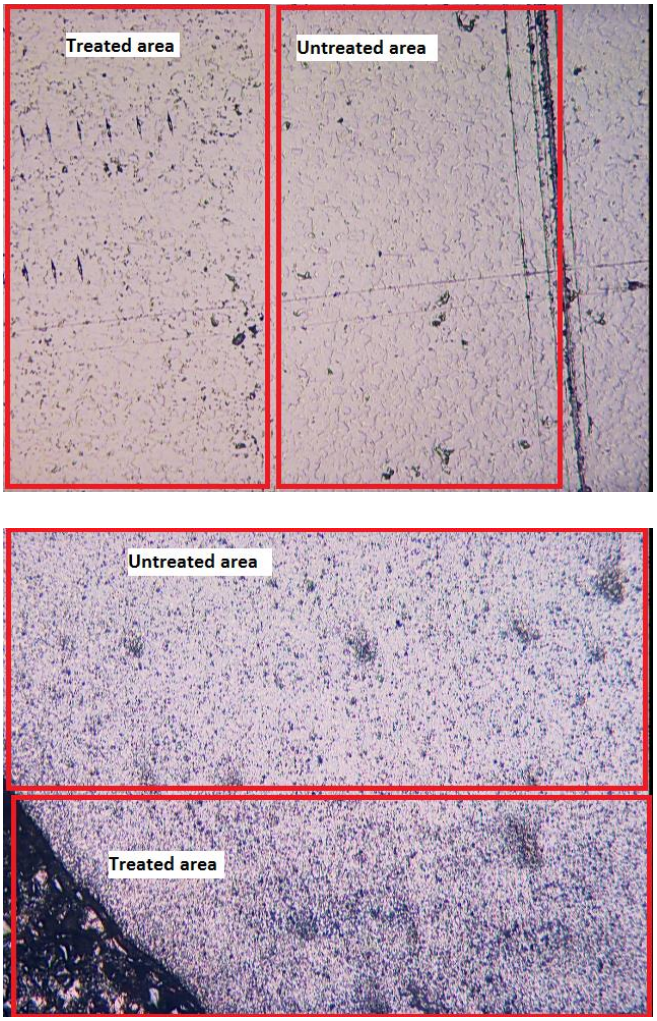

Figure 32: Comparison between untreated area and 2x2 mm treated area (top: 82% cBN, bottom: 55% cBN)

In the untreated area of the bindered 82%cBN/18%AlN sample, Raman spectrum showed two cBN peaks, which were 1059 and 1310 cm^{-1} (Figure 33). These two peaks can be considered as transverse optical (TO) and longitudinal optical branches of cBN. The position of Raman peaks and full width at half maximum (FWHM) of the cBN materials depends on impurities, defects, residual stress and grain size[51]. After the laser heat treatment, Figure 34 showed that the Raman peak of cBN phase moved slightly to 1056 and 1307 cm^{-1}.

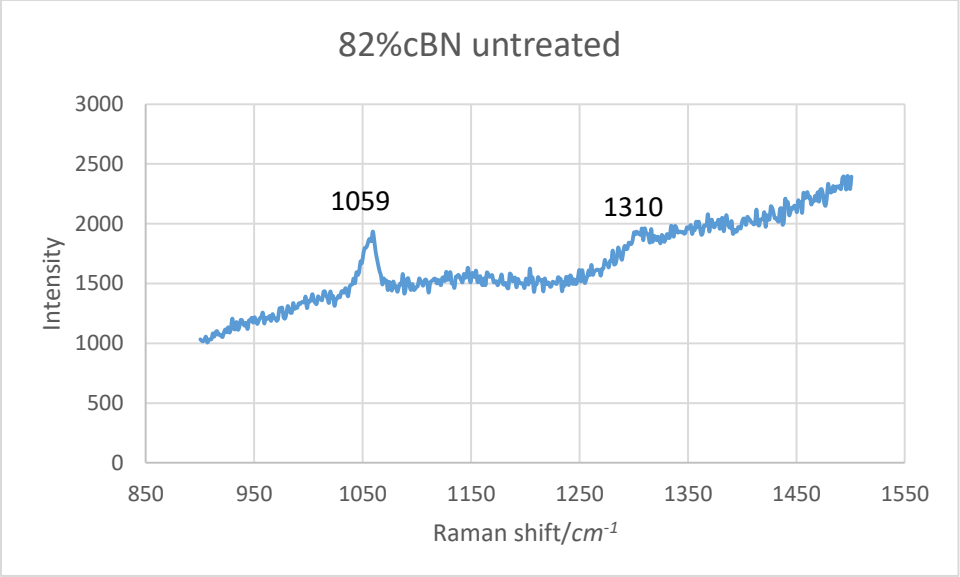

Figure 33: Raman spectrum of untreated 82% cBN

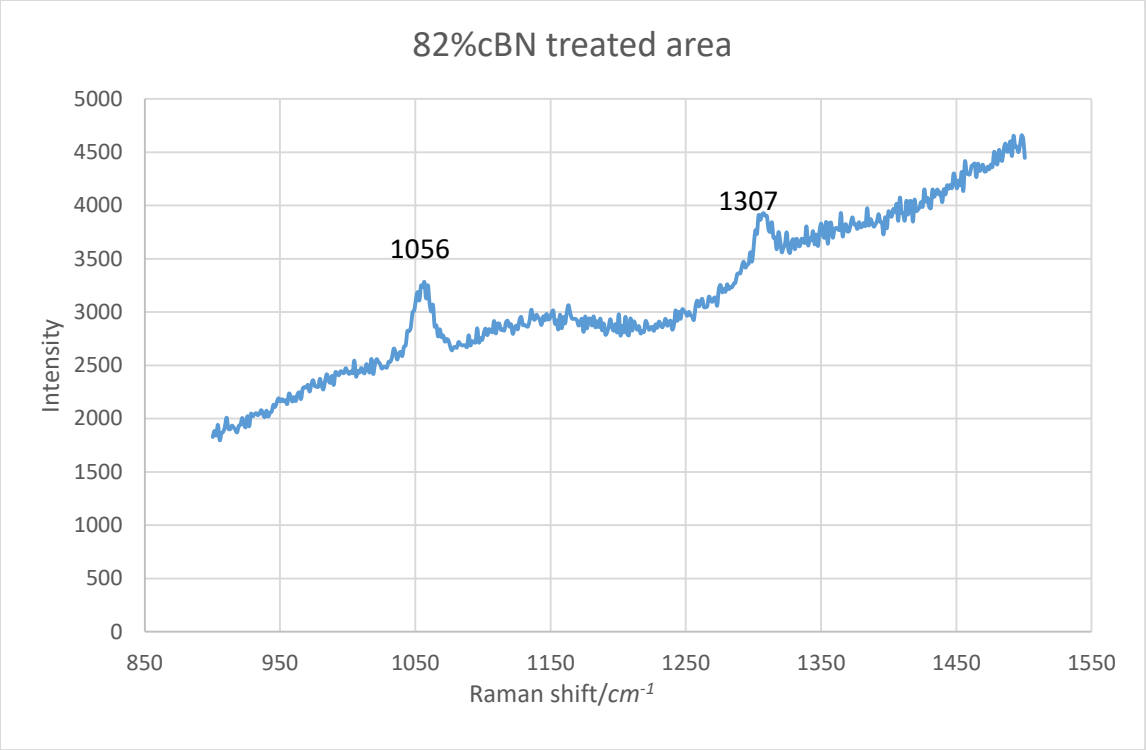

Figure 34: Raman spectrum of heat treated 82% cBN

On the other hand, Figure 35 showed the Raman peaks, which were 1082 (TO) and 1328 cm^{-1} (LO), in the untreated area of the bindered 55%cBN/45%Ti sample. After the laser heat treatment, the TO peak moved to 1077 cm^{-1} and the LO peak moved to 1338 cm^{-1}. Compared to the Raman spectrum of the bindered 82%cBN/18%AlN sample, the Raman spectrum of the bindered 55%cBN/45%Ti sample showed more background noise, so both the TO and LO peaks did not shift towards the same direction. The shifted and broadened peaks can be attributed to the plastic deformation caused in the heat treatment [51].

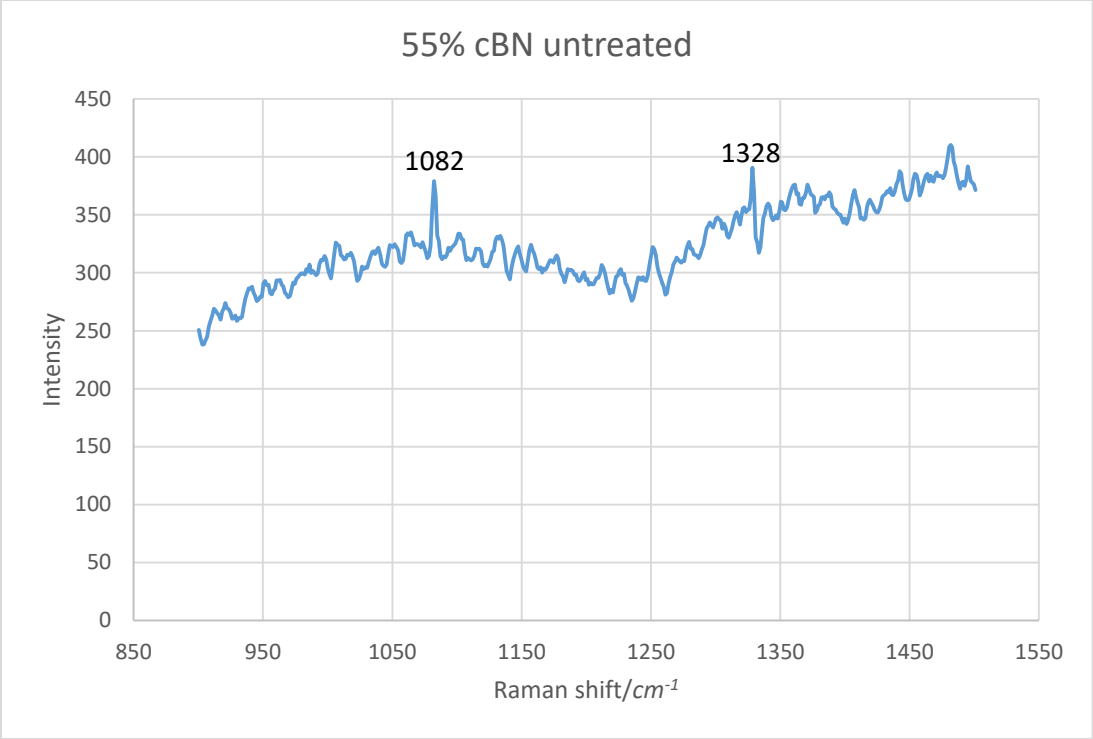

Figure 35: Raman spectrum of untreated 55% cBN

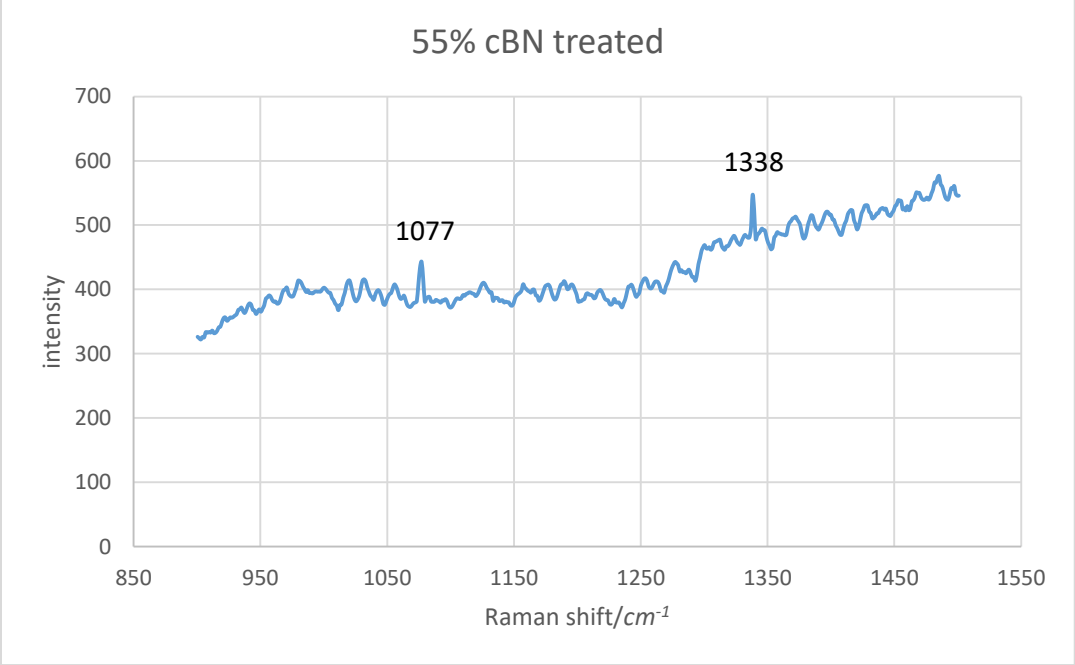

Figure 36: Raman spectrum of treated 55% cBN

3.5 Conclusions

In the experiment which included multiple laser beam passes on a single line, a significant increase in hardness was found in both samples. In the sample of bindered 82%cBN/18%AlN, an increase of about 20% in hardness was found in the 8-pass level. Furthermore, in the sample of bindered 55%cBN/45%Ti, the highest hardness increase of 18% was found in the 4-pass level. Therefore, 4-pass level was chosen for the second set of experiments.

Even though the 4-pass level fluence contributed the best performance in the single-line treatment, when used to treat the 2x2 area, there was a 3% lower increase in hardness may prove that this fluence is not the most suitable for use in treating the 2x2 mm area. However, since the hardness increase of the 2x2 mm treated area was close to the hardness increase of the single line, it indicates the feasibility of treating an area by using this method on cutting tools in order to increase their hardness.

In future works, different types of gases, such as nitrogen, argon, and oxygen, could be used as environmental gases in place of the water cover. The idea is that these environmental gases may allow a better coupling of laser energy to the material surface. Besides the environmental gases, the topic of different pulse widths of lasers is also interesting. The lasers with short pulse widths may cause a smaller heat-affected zone and less damage to the material surface.

CHAPTER 4: CONCLUSIONS AND FUTURE WORKS

4.1 Conclusions

Laser heat treatment using the LWJ system:

The hardness increase of the ultrahard material, cubic boron nitride, was found on different treated areas of passes. In the previous studies, the hardness of cBN increased up to 30% under the condition of using compressed air as the assisted gas and no microcrack were found on the sample surface. In my work with nitrogen as assisted gas, on the other hand, a 15% hardness increase was found and microcracks were found everywhere on the sample surface. Compared to the experiment with compressed air, a lower increase in hardness resulting from using nitrogen gas could contribute to the microcracks

Laser heat treatment using a pulsed laser system:

Hardness increases of 20% and 18% were found for two different compositions of cBN. In the experiments with water used as the medium, a higher hardness increase was found, compared to the experiments which did not use water. Therefore, the quenching effect was proven to be helpful in laser heat treatment. Furthermore, the microstructures of the untreated and heat-treated areas were also studied using SEM. In the treated areas, the grain size of BN was found to be smaller and the number of BN particles was found to be higher.

4.2 Future works

Laser heat treatment using the LWJ system:

Since Melaibari found that oxygen and argon as assisted gases contribute different results in machining [16], these two gases could be used to investigate the hardness and microstruture changes in cBN to see if they affect similar changes. Other experimental patterns can also be introduced, such as overlapping.

Laser heat treatment using pulsed laser system:

Instead of using a nanosecond laser, picosecond and femtosecond lasers can be used to study the mechanism of heat treatment on ultrahard materials. It is productive to investigate the feasibility of applying a shorter pulse width laser because it contributes a smaller heat-affected zone, compared to a longer width pulse laser. In all future studies, a greater increase in hardness will be a goal.

REFERENCES

1. Chandler, H., *Introduction to hardness testing.* Mechanical testing and evaluation, 2nd Edition, ASM International, 1999.
2. Maryland, C.a.t.U.o. *Material Hardness*. 2001; Available from: http://www.calce.umd.edu/TSFA/Hardness_ad_.htm.
3. Heath, P., *Ultra-hard materials.* European Journal of Engineering Education, 1987. **12**(1): p. 5-20.
4. Spriggs, G.E., *13.5 Properties of diamond and cubic boron nitride.* SpringerMaterials, 2002. **The Landolt-Börnstein Database**.
5. Wentorf Jr, R., *Synthesis of the cubic form of boron nitride.* The Journal of Chemical Physics, 1961. **34**(3): p. 809-812.
6. Cook, B., et al., *A new class of ultra-hard materials based on AlMgB 14.* Scripta Materialia, 2000. **42**(6): p. 597-602.
7. Ulrich, S., et al., *Subplantation effect in magnetron sputtered superhard boron carbide thin films.* Diamond and related materials, 1998. **7**(6): p. 835-838.
8. Basu, B., G. Raju, and A. Suri, *Processing and properties of monolithic TiB2 based materials.* International materials reviews, 2006. **51**(6): p. 352-374.
9. Photonics, R., *continuous-wave operation.* Encyclopedia of Laser Physics and Technology - continuous-wave operation, cw, 2017.
10. Patel, C.K.N., *Continuous-Wave Laser Action on Vibrational-Rotational Transitions of C O 2.* Physical review, 1964. **136**(5A): p. A1187.
11. Liu, X., D. Du, and G. Mourou, *Laser ablation and micromachining with ultrashort laser pulses.* IEEE journal of quantum electronics, 1997. **33**(10): p. 1706-1716.
12. Kumpulainen, T., et al., *Low temperature nanoparticle sintering with continuous wave and pulse lasers.* Optics & Laser Technology, 2011. **43**(3): p. 570-576.
13. Dahotre, N.B. and S. Harimkar, *Laser fabrication and machining of materials*. 2008: Springer Science & Business Media.
14. Willmott, P. and J. Huber, *Pulsed laser vaporization and deposition.* Reviews of Modern Physics, 2000. **72**(1): p. 315.
15. Perry, M., et al., *Ultrashort-pulse laser machining.* Lawrence Livermore National Laboratory, 1998.
16. Melaibari, A., P. Molian, and P. Shrotriya, *EFFECT OF FLUID MEDIUM ON LASER MACHINING OF POLYCRYSTLINE CUBIC BORON NITRIDE TOOL.* Lasers processing of ultra-hard materials, 2015. **1**: p. 9.
17. Cheng, G.J., et al., *Plastic deformation in silicon crystal induced by heat-assisted laser shock peening.* Journal of Manufacturing Science and Engineering, 2008. **130**(1): p. 011008.
18. Molian, P., *3D Printing of Nanoscale Powders using Laser Shock Waves.* Journal of Micro and Nano-Manufacturing, doi, 2015. **10**(1.4031462).
19. Baerga, R. and V. Orlando, *Laser shockwave sintering of micro and nanoscale powders of yttria-stabilized zirconia.* 2010.
20. Lim, H., et al., *Enhancement of abrasion and corrosion resistance of duplex stainless steel by laser shock peening.* Journal of Materials Processing Technology, 2012. **212**(6): p. 1347-1354.

21. Mondal, A., et al., *Effect of laser surface treatment on corrosion and wear resistance of ACM720 Mg alloy.* Surface and Coatings Technology, 2008. **202**(14): p. 3187-3198.
22. Badekas, H., C. Panagopoulos, and S. Economou, *Laser surface-treatment of titanium.* Journal of materials processing technology, 1994. **44**(1-2): p. 54-60.
23. Dubrovinskaia, N., et al., *Superhard nanocomposite of dense polymorphs of boron nitride: Noncarbon material has reached diamond hardness.* Applied Physics Letters, 2007. **90**(10): p. 101912.
24. Kalyanasundaram, D., et al., *Design and validation of a hybrid laser/water-jet machining system for brittle materials.* Journal of Laser Applications, 2008. **20**(2): p. 127-134.
25. Veprek, S., et al., *Superhard nanocomposites: Origin of hardness enhancement, properties and applications.* Surface and Coatings Technology, 2010. **204**(12-13): p. 1898-1906.
26. Veprek, S. and A.S. Argon, *Towards the understanding of mechanical properties of super- and ultrahard nanocomposites.* Journal of Vacuum Science & Technology B: Microelectronics and Nanometer Structures, 2002. **20**(2): p. 650.
27. Richard B. Kaner, J.J.G., Sarah H. Tolbert, *Designing Superhard Materials.* Science, 2005. **308**: p. 1268-1269.
28. Vepřek, S., *The search for novel, superhard materials.* Journal of Vacuum Science & Technology A: Vacuum, Surfaces, and Films, 1999. **17**(5): p. 2401.
29. U. Kuhlmann, H.W., T. Lundström, W. Robers *Optical properties of amorphous boron.* Journal of Physics and Chemistry of Solids, 1994. **55**(7): p. 579-587.
30. Melaibari, A.A., et al., *Ultrahard boron nitride material through a hybrid laser/waterjet based surface treatment.* Acta Mater, 2016. **102**: p. 315-322.
31. Jiménez, I., Sutherland, D., van Buuren, T., Carlisle, J., Terminello, L., & Himpsel, F., *Photoemission and x-ray-absorption study of boron carbide and its surface thermal stability.* Physical Review B, 1998. **57**(20): p. 13167–13174.
32. Riedel, R., *Novel ultrahard materials.* Advanced Materials, 1994. **6**(7-8): p. 549–560.
33. Basu, B., G.B. Raju, and A.K. Suri, *Processing and properties of monolithic TiB2based materials.* International Materials Reviews, 2013. **51**(6): p. 352-374.
34. Guo, X., et al., *Theoretical hardness of the cubic BC2N.* Diamond and Related Materials, 2007. **16**(3): p. 526-530.
35. Dubrovinskaia, N., S. Dub, and L. Dubrovinsky, *Superior wear resistance of aggregated diamond nanorods.* Nano Lett, 2006. **6**(4): p. 824-6.
36. Stan Vepreka, A.S.A., *Mechanical properties of superhard nanocomposites.* Surface and Coatings Technology 2001(146–147): p. 175–182.
37. Melaibari, A., P. Molian, and P. Shrotriya, *Laser/waterjet heat treatment of polycrystalline cubic/wurtzite boron nitride composite for reaching hardness of polycrystalline diamond.* Materials Letters, 2012. **89**: p. 123-125.
38. Kalyanasundaram, D., P. Shrotriya, and P. Molian, *Obtaining a Relationship Between Process Parameters and Fracture Characteristics for Hybrid CO[sub 2] Laser/Waterjet Machining of Ceramics.* Journal of Engineering Materials and Technology, 2009. **131**(1): p. 011005.
39. Chen, S.-L., *The effects of high-pressure assistant-gas flow on high-power CO2 laser cutting.* Journal of Materials Processing Technology 1999(88): p. 57–66.

40. Melaibari, A.A., *Lasers processing of ultra-hard materials.* Dissertations & Theses, 2015.
41. Jingnan Zhao, P.S., *Ultrahard Polycrystalline Cubic Boron Nitride Composite through Hybrid Laser:Waterjet Heat (LWH) Treatment* Procedia Manufacturing, 2016. **5**: p. 747-760.
42. Angseryd, J., et al., *Detailed microstructure of a cBN based cutting tool material.* International Journal of Refractory Metals and Hard Materials, 2009. **27**(2): p. 249-255.
43. William D. Callister, J., *Materials Science and Engineering: An Introduction (7th edition).* John Wiley & Sons, Inc., 2007.
44. Hansen, N., *Hall–Petch relation and boundary strengthening.* Scripta Materialia, 2004. **51**(8): p. 801-806.
45. Hou, X.D., A.J. Bushby, and N.M. Jennett, *Study of the interaction between the indentation size effect and Hall–Petch effect with spherical indenters on annealed polycrystalline copper.* Journal of Physics D: Applied Physics, 2008. **41**(7): p. 074006.
46. He, W., S.D. Bhole, and D. Chen, *Modeling the dependence of strength on grain sizes in nanocrystalline materials.* Science and Technology of Advanced Materials, 2016. **9**(1): p. 015003.
47. Kalyanasundaram, D., P. Shrotriya, and P. Molian, *Obtaining a Relationship Between Process Parameters and Fracture Characteristics for Hybrid CO2 Laser/ Waterjet Machining of Ceramics.* Journal of Engineering Materials and Technology, 2009. **131**(1): p. 011005.
48. Anyalebechi, P., *Materials Science and Engineering Laboratory Manual.* School of Engineering, Padnos College of Engineering and Computing, Grand Valley State University, 2005: p. 98-101.
49. Zhao, J. and P. Shrotriya, *Ultrahard Polycrystalline Cubic Boron Nitride Composite through Hybrid Laser/Waterjet Heat (LWH) Treatment.* Procedia Manufacturing, 2016. **5**: p. 747-760.
50. Anyalebechi, P., *Essentials of materials science and engineering.* School of Engineering, Padnos College of Engineering and Computing, Grand Valley State University, 2005: p. 137-156.
51. Melookaran, R., et al., *Laser shock processing on microstructure and hardness of polycrystalline cubic boron nitride tools with and without nanodiamond powders.* Materials & Design, 2012. **35**: p. 235-242.